Circulating Tfh cell activation, serological memory and tissue compartmentalization shape human influenza-specific B cell immunity

Marios Koutsakos[1], Adam K. Wheatley[1], Liyen Loh[1], E. Bridie Clemens[1], Sneha Sant[1], Simone Nüssing[1], Annette Fox[1], Amy W. Chung[1], Karen L. Laurie[2], Aeron C. Hurt[2], Steve Rockman[1,3], Martha Lappas[4], Tom Loudovaris[5], Stuart I. Mannering[5], Glen P. Westall[6], Michael Elliot[7,8], Stuart G. Tangye[9,10], Linda M. Wakim[1], Stephen J. Kent[1,11,12], Thi H.O. Nguyen[1*] and Katherine Kedzierska[1*]

[1]Department of Microbiology and Immunology, University of Melbourne, at the Peter Doherty Institute for Infection and Immunity, Parkville 3010, Victoria, Australia.
[2]World Health Organisation (WHO) Collaborating Centre for Reference and Research on Influenza, at The Peter Doherty Institute for Infection and Immunity, Melbourne 3000, Victoria, Australia.
[3] Seqirus, 63 Poplar Rd, Parkville 3052, Victoria, Australia.
[4]Obstetrics, Nutrition and Endocrinology Group, Department of Obstetrics & Gynaecology, University of Melbourne, Mercy Hospital for Women; Heidelberg 3084, Victoria, Australia.
[5]Immunology and Diabetes Unit, St Vincent's Institute of Medical Research, Fitzroy 3065, Victoria 3065, Australia.
[6]Lung Transplant Unit, Alfred Hospital, Melbourne 3004, Victoria, Australia.
[7]Sydney Medical School, University of Sydney, Sydney;
[8]Chris O'Brien Lifehouse Cancer Centre, Royal Prince Alfred Hospital, Sydney
[9]Immunology Division, Garvan Institute of Medical Research, Darlinghurst 2010, New South Wales, Australia.
[10]St. Vincent's Clinical School, University of New South Wales, Sydney 2052, New South Wales, Australia.
[11]Melbourne Sexual Health Centre and Department of Infectious Diseases, Alfred Hospital and Central Clinical School, Monash University, Melbourne 3004, Victoria, Australia.
[12]ARC Centre for Excellence in Convergent Bio-Nano Science and Technology, University of Melbourne, Parkville 3010, Victoria, Australia.

*These authors contributed equally.
Corresponding authors: kkedz@unimelb.edu.au (K.K.); tho.nguyen@unimelb.edu.au (T.H.O.N.);

One Sentence Summary: Analysis of influenza-specific B cells during antigen exposure and tissue compartmentalization provide new insights into human B cell memory.

Abstract

Immunization with the inactivated influenza vaccine (IIV) remains the most effective strategy to combat seasonal influenza infections. IIV activates B cells and T follicular helper (Tfh) cells, and thus engenders antibody-secreting cells and serum antibody titres. However, the cellular events preceding generation of protective immunity are inadequately understood. We undertook an in-depth analysis of B cell and T cell immune responses to IIV in 35 healthy adults. Using recombinant hemagglutinin (rHA) probes to dissect the numbers, phenotype and isotype of influenza-specific B cells against A/California09-H1N1, A/Switzerland-H3N2 and B/Phuket, we showed that vaccination induced a three-pronged B cell response comprising a transient $CXCR5^{-}CXCR3^{+}$ antibody-secreting B cell population, $CD21^{hi}CD27^{+}$ memory B cells and $CD21^{lo}CD27^{+}$ B cells. Activation of circulating Tfh cells correlated with the development of both $CD21^{lo}$ and $CD21^{hi}$ memory B cells. However, pre-existing antibodies could limit increases in serum antibody levels. Strikingly, IIV had no marked effect on $CD8^{+}$, MAIT, γδ T cells and NK cell activation. Additionally, vaccine-induced B cells were not maintained in peripheral blood at one-year post-vaccination. Importantly, we provide the first dissection of rHA-specific B cells across seven human tissue compartments, showing that influenza-specific memory B cells primarily reside within secondary lymphoid tissues and the lungs. Our study suggests that a rational design of universal vaccines needs to consider circulating Tfh cells, pre-existing serological memory and tissue compartmentalization for effective B cell immunity, as well as to improve targeting cellular T cell immunity.

Introduction

Influenza remains a significant public health problem, causing seasonal annual epidemics, occasional widespread pandemics and sporadic outbreaks in animals. In humans, two influenza A virus (IAV) strains (H1N1 and H3N2) along with one influenza B virus (IBV), from either the Victoria and Yamagata lineage, co-circulate annually (*1*). Vaccination with an inactivated influenza virus is currently the most effective way of inducing strain-specific neutralizing antibodies directed against surface glycoproteins, hemagglutinin (HA) and neuraminidase (NA). In the absence of antibody-mediated immunity, pre-existing memory B-cells (*2, 3*) and broadly cross-reactive memory T-cells (*4-6*) can be recalled and protect against influenza. Due to the antigenic drift of IAV and IBV, and antigenic shifts of IAV, memory B-cell and T-cell populations are central for controlling antigenically-distinct influenza strains. Thus, effective influenza vaccines need to establish long-lasting memory B-cells and T-cells, readily recalled during infection with novel influenza viruses.

Following antigen re-exposure, memory B-cells develop into short-lived effectors (plasmablasts and plasma cells, jointly named as antibody-secreting cells; ASCs) and rapidly provide antibodies. Additionally, memory B-cells re-enter germinal centers, resulting in generation of affinity-matured long-lived plasma cells (LLPCs) and memory B-cells (*7, 8*). This process depends on co-stimulation and cytokine production by T follicular helper (Tfh) cells (*9, 10*). Following IIV, a transient population of ASCs, predominantly derived from memory B-cells, emerges in peripheral blood on day (d) 7 after vaccination and correlates with antibody titres (*2, 11*). Concomitantly, a population of circulating Tfh (cTfh; $CD4^+CXCR5^+$) cells (*12*) also emerges in peripheral blood on d7 post-vaccination (*13*). These cTfh cells exhibit a type-1 phenotype ($CXCR3^+CCR6^-$), express activation markers (ICOS and PD-1), provide help to memory (but not naïve) B-cells for development into ASCs and correlate with ASCs and antibody responses (*13*). However, the role of human cTfh cells in establishing B-cell memory is not entirely understood. Recent studies described new subsets of antigen-specific B-cells, based on the expression of CD21 and CD71, emerging with variable dynamics following immunization (*14, 15*). Additionally, influenza exposure history and pre-existing antibodies can shape the antibody response to IIV (*16-18*), although mechanisms are ill-defined. Important questions remain with regards to the generation and maintenance of immune memory B-cells and T-cells following IIV.

We dissected cellular events that precede the serological response to IIV and showed that vaccination induces a robust population of cTfh cells, important for subsequent immunological events, specifically seroconversion and the emergence of three influenza-specific (defined by rHA probes) B-cell populations: ASCs, $CD21^{lo}$ and $CD21^{hi}$ memory B-cells. We provided the data on distribution of rHA-specific B-cells across seven human tissues and demonstrate that IIV did not affect $CD8^+$ or innate T-cells. The key findings of our studies are that (i) the emergence of cTfh1 cells on d7 correlates with the magnitude of memory B-cell response on d14; (ii) serological memory on d0 limits the development of $CD21^{lo}$ memory B-cells; (iii) influenza-specific memory B-cells are differentially distributed across human tissues, with memory rHA-specific B-cells being enriched in secondary lymphoid organs and the lung. These findings have fundamental implications for the rational design of vaccines that induce protective and long-lasting immunity against influenza viruses.

Results

Influenza vaccination induces activation of circulating Tfh cells and expansion of $CXCR3^+CXCR5^-$ antibody-secreting cells

To dissect the cellular events preceding generation of protective immunity to IIV, blood samples were obtained from healthy adults at baseline (BL), d7, d14 and d28 after intramuscular immunization. Our study involved 35 vaccinees over three years, with a total sample size of 42 (Table S1). A/California/7/2009 remained constant throughout three years of vaccination, while A/H3N2 and IBV components were updated annually to reflect antigenically-drifted A/H3N2 strains and circulating Yamagata or Victoria IBV viruses (Fig. 1A).

The kinetics of cTfh cells ($CD4^+CXCR5^+$) and ASCs ($CD19^+CD27^+CD38^{hi}$ B-cells) in peripheral blood were evaluated (fig. S1). After vaccination, the numbers of cTfh type-1 subset (cTfh1; $CXCR3^+CCR6^-$) expressing ICOS and PD-1 ($ICOS^+PD\text{-}1^+$cTfh1) significantly expanded ($p<0.0001$) on d7, before returning to baseline by d14 (Fig. 1B-C). The numbers of cTfh2 ($CXCR3^-CCR6^-$) and cTfh17 ($CXCR3^-CCR6^+$) cells did not increase following vaccination (fig S2A-B). We found increased ($p<0.0001$) frequency of activated $CD38^{hi}$ cells within $ICOS^+PD\text{-}1^+$cTfh1 set on d7 after vaccination (Fig. 1D-E). While CD38 expression was higher on cTfh2 and cTfh17 than on cTfh1 cells at baseline ($p<0.001$), cTfh1 cells had a higher CD38 mean fluorescence intensity (MFI) at d7 ($p<0.0001$) (fig. S2C). CD38 on d7 was higher on $ICOS^+PD\text{-}1^+$cTfh1 cells than on non-activated $ICOS^-PD\text{-}1^{+/-}$cTFh1 cells

(p=0.002) (fig. S2D). These data show that vaccination with IIV specifically activates cTfh1 cells.

As previously reported (*2, 11*), ASCs transiently appeared in blood (Fig. 1G) peaking on d7 following vaccination (p<0.0001 compared to baseline), then declining at d14 and d28 (Fig. 1F-G). We found a transient increase in expression of CXCR3 on ASCs on d7 (p<0.001) (Fig. 1H-I), not observed on non-ASC (non-$CD38^{hi}CD27^{+}$) B-cells (p<0.0001) (Fig. 1J). Additionally, while non-ASC B-cells expressed high levels of CXCR5, circulating ASCs lacked CXCR5 expression (p<0.0001) (Fig. 1K). Thus, circulating ASCs present in blood on d7 after vaccination display unique expression patterns of chemokine receptors, CXCR3 and CXCR5, important for trafficking of B-cells. Based on the HA inhibition assay (HAI), IIV also increased serum antibody titres (d28 compared to baseline) against A/H1N1, A/H3N2 and IBV components (Fig. 1L). These data show that IIV induces transient and concurrent changes in circulatory B-cell and Tfh compartments.

Detection of influenza-specific B-cells by recombinant hemagglutinin probes

To determine the numbers, phenotype and isotype of B-cells elicited by IIV, we identified influenza-specific B-cells with recently developed rHA probes (*19-21*), consisting of four biotinylated trimeric rHA molecules conjugated to streptavidin-fluorochrome complexes. To prevent non-specific binding to sialic acids, rHA probes contained mutations Y98F for IAV and T190G for IBV (*21*). We used rHA probes against three vaccine components, A/California/07/09-H1N1 (A/Cal09-H1), A/Switzerland/9715293/2013-H3N2 (A/Swi-H3) and B/Phuket/3073/2013 (BHA; Yamagata lineage) (Fig. 2A). Using PBMC from healthy adults, influenza probe-specific B-cells were identified within mature class-switched $CD19^{+}CD3^{-}CD14^{-}CD16^{-}CD10^{-}IgD^{-}$ B-cells, with exclusion of cells binding free fluorochrome-streptavidin (Fig. 2A; fig. S3).

We validated the specificity of rHA-probes for detection of influenza-specific B-cells, using different experimental approaches (figs S4-5). Dual rHA probe staining (two rHA-probes of the same specificity conjugated to different fluorochromes) (*22*) showed that the majority of class-switched IgD^{-} B-cells were double-positive (97%/90% for H1; 92%/50% for H3; 91%/86% for B, across APC- and PE-conjugated probes; fig S4A-B), reflecting high level of probe-specificity. Because of its higher sensitivity, our subsequent data were generated using the H3-APC probe. However, double-positive rHA staining within unswitched IgD^{+}B-cells was considerably lower (17-55% depending on the probe and

fluorochrome; fig S4A-B). Thus, we excluded them from our analyses because of high-level non-specific rHA binding.

Secondly, we blocked rHA staining with sheep anti-HA sera against each of the probes. Blocking with cognate anti-sera specifically reduced rHA staining on class-switched B-cells by 82-93% (fig S4C-D), further demonstrating specificity of rHA-biding to IgD^-B-cells.

We also single-cell FACS-sorted $CD19^+IgD^-IgM^-IgG^+CD27^+rHA^+$ B-cells directly *ex vivo* from PBMCs. BCR heavy chain sequences for rHA-$H1^+$ and rHA-B^+ B-cells were recovered using a multiplex PCR approach (*23*). A high proportion of BCR sequences (57% for rHA-H1+; 65% for rHA-B^+ B-cells) exhibited clonal expansions (same IGHV usage and CDR3 homology) (fig S5A), a reliable indicator of antigenic-specificity. Furthermore, distribution of clonal sizes showed typical distributions of clones, with 1-2 largely-expanded clones, 10-11 medium-size clones, 16-23 small clones and a natural tail of 83-97 singletons (fig S5B). As clonality is a function of a sequencing depth, some of the singletons would be also HA-specific. Additionally, our data show that the rHA-specific singletons utilize the same heavy chain segments as the largely-expanded clones (fig S5c), suggesting their specificity. Overall, rHA^+ probes for detection of influenza-specific IgD-B-cells were validated using dual-probe staining, blocking with sheep anti-sera and BCR sequencing.

At steady state, the numbers of peripheral blood A/Cal09-$H1^+$ B-cells (median 40.3 cell/ml blood) were significantly higher than A/Swi-$H3^+$ (median 22.5 cells/ml blood) and B/Phu-HA^+ B-cells (median 24.2 cells/ml blood) (Fig. 2B). Influenza-specific B-cells were grouped according to their isotype as IgG^+, IgA^+ and IgM^+ subsets (fig. S3). Although anti-IgA staining was not included due to the limited capacity of flow cytometry, our separate analysis showed that 100% (n=25, fig. S6) of A/Cal09-$H1^+$ $IgG^-IgD^-IgM^-$ cells, were IgA^+ and hence $IgG^-IgD^-IgM^-$ were classified as IgA^+. While a larger proportion of B/Phu-HA^+ B-cells were IgG^+ (H1: median 74.2%, H3: 60.6%, B: 83.4%) (Fig 2C-D), in terms of numbers of B-cells/ml, there were more A/Cal09-$H1^+$ IgG^+ B-cells (Fig 2E). Accordingly, there were less IgA^+ or IgM^+ B/Phu-HA^+B-cells found than for the other two specificities. Analysis of the memory CD27 and activation CD21 (complement receptor 2) markers to identify resting memory B-cells ($CD21^{hi}CD27^+$) (fig. S3) showed that the three rHA^+ populations exhibited similar phenotype distributions, with resting memory B-cells being the most prominent (H1: median 50%, H3: 48%, B: 55.2%) (Fig 2H-I). A/Cal09-$H1^+$ $CD21^{hi}CD27^+$ B-cells were the most prominent (H1: median 18.5 cells/ml, H3: 11 cells/ml, B: 12.2 cells/ml) (Fig 2J),

reflecting their greater abundance. Overall, while the IAV-H1$^+$B-cell pool is larger in size, the IBV-specific B-cell pool contains more IgG$^+$B-cells.

CD21^{hi}CD27$^+$ and CD21^{lo}CD27$^+$ influenza-specific B-cells emerge in peripheral blood after vaccination

To determine how the rHA$^+$B-cell pool responds to IIV, we assessed numbers and phenotype of influenza-specific B-cells following vaccination in 2015 and 2016 cohorts. While A/Cal09-H1 was constant across both years, the H3 component was updated in 2016 with the A/Hong Kong strain, belonging to the same clade (3C) but a different subclade (3C.2a) to the A/Switzerland strain (3C.3a). As an A/Hong Kong rHA probe was unavailable, samples from the 2016-cohort were stained with the heterologous A/Swi-H3 probe. For IBV, the B/Phuket (Yam) strain was present in IIV in both years, as a sole IBV component in 2015, and together with the B/Brisbane (Vic) in 2016 as a part of the quadrivalent formulation. B/Phuket-specific B-cells were analysed during 2015 and 2016, while a probe for B/Brisbane was unavailable.

Vaccination significantly increased the numbers of B-cells specific for three IIV components (Fig. 3A-B). This increase was observed on d7, peaked at d14 and was maintained until d28. Thus, IIV increases the size of the influenza-specific B-cell pool, at least until d28 after immunization. Additionally, a subset of B-cells specific for each of the vaccine components transiently acquired an ASC-like phenotype (CD27^{hi}CD20^{lo}) on d7 (Fig. 3C-D). Following vaccination, IgG$^+$, IgA$^+$ and IgM$^+$ influenza-specific B-cells underwent significant expansion (Fig. 3E). The response was mainly dominated by IgG$^+$ B-cells, with a median of 63.7 A/Cal09-H1$^+$ cells/ml, 36.7 A/Swi-H3$^+$ cells/ml and 24.2 BHA$^+$ cells/ml of blood on d14, and a smaller IgA$^+$ population (14.9 A/Cal09-H1$^+$ cells/ml, 12.5 A/Swi-H3$^+$ cells/ml and 7.9 BHA$^+$ cells/ml). Although minimal, significant changes were observed for IgM$^+$rHA$^+$ B-cells. For H3, HA-specific B-cell patterns were similar when data were analyzed from both the 2015-cohort (using a homologous probe), and the 2016-cohort (using a heterologous probe) together (Fig. 3B) or separately (fig. S7), reflecting the effect of back-boosting and recall of memory B-cells. To confirm the data obtained by rHA staining, we used polyclonal stimulation and a B-cell ELISPOT assay (fig S8). While at baseline B-cells against A/Cal09 H1 and B/Phu were undetectable, B-cells against both strains increased at d14 (fig S8A), similarly to measurements by FACS (fig S8B). Importantly, the number of IgG$^+$rHA$^+$B-cells correlated ($r=0.7$, $p=0.0005$) with the number of IgG$^+$ spot-forming units (SFU/million PBMC) (pooled data for H1 and B from d0 and d14), supporting our analysis

by rHA probes.

Further phenotyping of rHA^+IgG^+ B-cells revealed that while these cells predominantly displayed a resting memory phenotype ($CD21^{hi}CD27^+$) at baseline, HA-specific B-cells across all vaccine components transitioned to an activated memory phenotype ($CD21^{lo}CD27^+$) from d7 until d28, with a noticeable peak on d14 (Fig. 3F-G). The $CD21^{lo}$ B-cell population was distinct from the ASC phenotype, as the latter cells were $CD20^+$ (fig. S9). Overall, IIV increased the numbers of $CD21^{hi}$ and $CD21^{lo}$ IgG^+ influenza-specific B-cell pool, both of which peaked on d14 for IgG^+B-cells.

Activation of cTfh1 cells correlates with increased numbers of $CD21^{hi}CD27^+$ and $CD21^{lo}CD27^+$ HA-specific B-cells in the periphery

We found four key effector cells in the immune response to IIV: ASCs and activated cTfh1 cells, transiently emerging in the circulation on d7, $CD21^{hi}CD27^+$ and $CD21^{lo}CD27^+$ influenza-specific B-cells, peaking on d14. We further investigated how these cellular events are interlinked and how they relate to the magnitude of the serological response. As the 2016 vaccine formulation included a new H3N2 strain and a second IBV strain, for which rHA^+ probes were unavailable, the analysis focused on the 2015-cohort (n=16). For other analyses, pooled data from the 2015- and 2016-cohort (n=42) were used.

A correlation between the number of blood ASCs/µl on d7 and the antibody response following IIV (total fold-change on d28 over d0) (r_s=0.37, p=0.013) was found (Fig. 4A). The total fold-increase was defined as the sum of the fold-change for all the vaccine components, as the cTfh1 and ASCs detected on d7 could not be attributed to a specific vaccine component. Accordingly, individuals who seroconverted following IIV (≥four-fold change in HAI titers to at least one vaccine component) had a significantly higher ASCs/µl numbers at d7, as compared to non-seroconverters (p=0.0381) (Fig. 4B), as in studies showing that the serological response to vaccination was linked to the emergence of ASCs (*2,24*). Indeed, in the 2014-cohort with longitudinal serum samples, the HAI titre increased as early as d7 (Fig. 4C), suggesting that the serological response observed following vaccination is derived from this transient ASC population.

Similarly, $ICOS^+PD\text{-}1^+$cTfh1 cells showed a moderate correlation with the total fold-increase in HAI titres (r_s=0.43, p=0.0042) (Fig. 4D). Notably, seroconverters had a higher number of $ICOS^+PD\text{-}1^+$cTfh1 cells, when compared to non-seroconverters (NS) (p=0.0328) (Fig. 4E). Additionally, the number of ASCs on d7 showed a moderate positive correlation with the number of $ICOS^+PD\text{-}1^+$cTfh1 cells on d7 (r_s=0.6307, p<0.0001) (Fig. 4F). Thus, the

emergence of activated cTFh1 cells, circulating ASCs and the antibody response on d7 are interlinked.

The number of $ICOS^+PD\text{-}1^+$cTfh1 cells on d7 also correlated with the fold-change in both $CD21^{hi}CD27^+$ (r_s=0.7353, p=0.0017) and $CD21^{lo}CD27^+$ IgG^+ memory B-cells specific for all vaccine components (r_s=0.7265, p=0.002) (Fig. 4G), highlighting a central role for cTfh1 cells in B-cell memory generation and seroconversion. Thus, the emergence of cTfh1 cells is important for the immune response to IIV as they are linked to the increase of ASCs and $CD21^{hi}CD27^+$ and $CD21^{lo}CD27^+$ HA-specific B-cell memory in the periphery.

Pre-existing antibodies negatively correlate with the serological response and the emergence of $CD21^{lo}CD27^+$ influenza-specific B-cells

Individuals who seroconverted to H1 and B had lower serum titres at baseline than those who did not respond to the vaccine (H1: p=0.0062, B: p=0.0045) (Fig. 5A), showing that seroconversion is influenced by pre-existing serum titres, as reported (*17*). This was not observed for H3N2 (p=0.29), which differed in both 2015 and 2016. Correspondingly, pre-existing titres to H1 and B components showed a negative correlation with the cognate fold-increase in HAI titres (H1: r_s=-0.5, p=0.0005, B: r_s=-0.55, p=0.0001) (Fig. 5B). This differed for the drifted H3 component (r_s=-0.29, p=0.06). When HAI titres against all vaccine components were added, there was a significantly strong negative correlation between the baseline HAI titres versus the fold-increase in HAI titres on d28/d0 (r_s=-0.56, p=0.0001) (Fig. 5C).

Conversely, the total pre-existing serum titres on d0 did not impact the emergence of total ASCs (r_s=0.063, p=0.69) (Fig. 5D) or $ICOS^+PD\text{-}1^+$cTfh1 cells (r_s=-0.02571, p=0.8716) (Fig. 5E) at d7. Additionally, pre-existing serum titres had no effect on the fold-change of memory $CD21^{hi}rHA^+$B-cells for either of the components (H1: r_s=-0.16, p=0.54, B: r_s=-0.12, p=0.67, H3: r_s=0.08, p=0.76) (Fig. 5F). However, pre-existing titres against B, but not H1 or H3, negatively correlated with the fold-change of cognate $CD21^{lo}rHA^+$B-cells (H1: r_s=-0.35, p=0.2, B: r_s=-0.76, p=0.0015, H3: r_s=-0.0045, p=0.992) (Fig. 5G). Thus, pre-existing serological memory can limit seroconversion and the magnitude of $CD21^{lo}$B-cells.

Vaccination with IIV does not induce $CD8^+$ and innate T-cells

To determine the effect of IIV on cellular immunity, we examined influenza-specific $CD8^+$ T-cells, $CD4^+$ T-cells, γδ T-cells, mucosal-associated invariant T (MAIT) cells and natural killer (NK) cells, assessed by intracellular cytokine staining (ICS) for IFNγ and TNF

following an *ex vivo* overnight stimulation with IAV and IBV (A/Cal09 H1N1pdm09, B/Phuket) in 7 donors vaccinated in 2015 (fig. S10). The frequency and numbers of IFNγ^{+}CD8^{+} T-cells, γδ T-cells, MAIT-cells and NK cells remained unchanged in response to IAV and IBV, with no apparent differences between the pre- and post-vaccination time-points (Fig. 6A-B and fig. S11). Consistent with previous studies, IFNγ^{+}CD4^{+}T-cells increased in response to IAV (not IBV) at d14 (median d0: 819 cells/µl blood, d14: 1129 cells/µl blood, p=0.038), although this increase was not maintained at d28. To further probe any effects of IIV on CD8^{+}T-cells, we used fluorochrome-conjugated peptide/MHC-I tetramers for IAV-derived epitopes (A2-M1$_{58-66}$, A1-NP$_{44-52}$ and B8-NP$_{225-233}$) in 3 donors (fig. S12). Consistent with the ICS, vaccination did not alter the frequencies (Fig. 6C-D) or differentiation status (CD27/CD45RA phenotype) (Fig. 6E-F) of tetramer^{+}CD8^{+}T-cells. Lastly, there were no differences in the expression of differentiation (CD27/CD45RA), activation (HLA-DR/CD38), proliferation (Ki-67) markers (Fig. 6G) or the effector granzyme-B on T-cells (n=14) (fig. S12). Overall, influenza-specific T-cell compartments (with the exception of CD4^{+}T-cells) remains unchanged following IIV.

Vaccine-induced memory B-cells are not maintained in peripheral blood

For vaccine-induced immunity to be protective, it needs to be long-lived. We assessed the longevity of vaccine-induced influenza-specific antibodies and B-cells. Serum titres (but not influenza-specific B-cells) for the three vaccine components were stable (within the four-fold difference) over the one-year period (>350 days) post-vaccination (Fig. 7AB). However, when the isotype distributions for vaccine components were analysed, a loss of vaccine-induced IgG^{+} and IgA^{+} rHA^{+}B-cells was observed at one year (Fig. 7C-D). This loss was pronounced and significant when IgG^{+}CD21^{hi} and IgG^{+}CD21^{lo} rHA^{+}B-cells were analysed (Fig. 7E), suggesting that the vaccine-induced influenza-specific memory B-cells are not maintained in peripheral blood.

As eight individuals received IIV vaccination in two consecutive years, we analysed rHA^{+}IgD^{-}B-cells within these individuals across different years. Overall, total IgD^{-}rHA^{+}B-cell and CD21^{hi} and CD21^{lo} CD27^{+}rHA^{+} responses were comparable across repeated vaccinations (Fig 7 F-G). However, when the fold-change over its respective baseline for each year was calculated, B-cell responses peaked earlier (at d7) in the second year and the responses were larger (fig S13). While these findings are interesting, the small number of donors and the lack of a vaccination history precluded us from further dissecting the effects of previous vaccination on influenza-specific B-cell responses.

B-cells show distinct patterns of tissue compartmentalization

As the loss of vaccine-induced B-cell memory in blood could result from transition between phenotypes, contraction of vaccine-induced B-cell pools or migration of memory B-cells into tissues, we analysed the distribution and phenotype of total and influenza-specific B-cells across seven human tissue compartments. Spleens, lungs and lymph nodes were obtained from deceased organ donors, while peripheral blood, bone marrow, cord blood and tonsils were obtained from healthy individuals. B-cells were phenotypically divided into four populations based on the expression of CD27 and CD21. Naïve B-cells were defined as $CD21^{hi}CD27^{-}$, resting memory as $CD21^{hi}CD27^{+}$, activated memory as $CD21^{lo}CD27^{+}$ and tissue-like (atypical) memory as $CD21^{lo}CD27^{-}$. Dual rHA probe staining confirmed the probe specificity in tissues (spleen and lung) as the majority of $rHA^{+}IgD^{-}$B-cells were double-positive (91%/71% for H1; 93%/71% for H3; across APC/PE-conjugated probes; fig S14A-B).

Total mature $CD19^{+}CD3^{-}CD14^{-}CD16^{-}CD10^{-}$B-cells were enriched in secondary lymphoid tissues (SLOs), with a median of ~50% lymphocytes being B-cells in the tonsils, lymph nodes and spleen, as compared to 6.5% in adult blood, 13.7% in cord blood, 11.1% in bone marrow and 4.8% in the lung (Fig. 8A). Naïve B-cells ($CD21^{hi}CD27^{-}$) were found in human tissues, alongside the other B-cell subsets (Fig. 8B). The majority of naïve B-cells was detected in cord blood (86.4%) and bone marrow (88.3%), consistent with the lack of antigen exposure in cord blood and the development of B-cells in the bone marrow. ~75% of blood and tonsil B-cells were unswitched, while the spleen and lymph nodes contained a higher proportion of resting memory B-cells (48.2% and 63.3%). The human lung contained 52.4% resting memory B-cells and 38.6% unswitched B-cells. Activated memory ($CD21^{lo}CD27^{+}$) B-cells were infrequent, consistent with the donors' healthy status. Similar results were obtained from isotype analysis across human tissues (Fig. 8C). $IgD^{+}M^{+}$B-cells were the predominant subset across tissues, followed by $IgD^{+}M^{-}$B-cells and then class-switched B-cells (IgG^{+}, IgA^{+}, IgM^{+}). IgA^{+}B-cells and IgM^{+}B-cells were most prevalent in the lymph node, spleen and lung.

Influenza-specific class-switched B-cells (A/Cal09-$H1^{+}$, A/Swi-$H3^{+}$) were readily detected in all tissues (Fig. 8D). The frequency of rHA^{+}B-cells ranged from 0.029% to 0.4% of IgD^{-}B-cells. Furthermore, while the frequency of $rHA^{+}IgD^{-}$ cells within B-cells was similar across tissues, $rHA^{+}IgD^{-}$ B-cells within lymphocytes were more abundant in SLOs

(tonsils, lymph nodes, spleen) than other tissues. While in blood only 39.8% of $rHA^{+}IgD^{-}$B-cells were $CD27^{+}CD21^{hi}$, there was an enrichment of $CD27^{+}CD21^{hi}rHA^{+}$B-cells in all tissues (mean 80.9-98%) (Fig 8E). While $IgG^{+}rHA^{+}$B-cells were more prominent in the circulation (mean 87.9%), this was lower in tissues (50.4-70.9%). Instead, tissues showed larger proportions of IgM^{+} and IgA^{+} rHA^{+}B-cells (Fig 8F). Overall, influenza-specific B-cell memory is compartmentalized outside of peripheral blood.

To normalize for differences between donors due to exposure history and age, we analyzed B-cell tissue compartmentalization in paired peripheral blood and spleen samples (n=5, table S2). Analysis of total B-cells confirmed enrichment of $CD21^{hi}CD27^{+}$ memory in the spleen compared to blood (Fig 8H) and differential distribution of different isotypes between blood and tissues (fig. S15). Due to the low cell numbers available, we could not confidently detect influenza-specific B-cells.

Discussion

Vaccination with inactivated influenza remains the predominant prophylactic measure against infection. Understanding the cellular events that precede the induction of protective immunity is pivotal in the development of better vaccines. We provide a comprehensive analysis of the immune response to vaccination in healthy individuals. Using rHA probes to characterize influenza-specific B-cells, we show that vaccination induces an early wave of influenza-specific short-lived effectors (ASCs), accompanied by an increase in antibody titres, and a second wave of $CD21^{hi}CD27^{+}$ and $CD21^{lo}CD27^{+}$B-cells. Concomitantly, activated cTfh1 cells correlated with all arms of this response. Vaccine-induced B-cells were not maintained in peripheral blood and overall, human memory B-cells were enriched in SLOs and peripheral tissues. Strikingly, vaccination had no impact on $CD8^{+}$ and innate T-cells. Our study provides insights into the human B-cell response and recapitulates fundamental aspects of B-cell biology from animals, translating them into humans across different tissues.

Previously, ASCs on d7 correlated with seroconversion (*2, 24*). Our kinetic data and correlation analyses support this model. Consistent with studies in mice (*25, 26*) and tetanus vaccination in humans (*27*), our findings show that the emergence of ASCs is accompanied by a chemotactic switch, specifically the loss of CXCR5, releasing B-cells from germinal centers and preventing their re-entry, and upregulation of CXCR3, directing them to sites of inflammation and likely the bone marrow (*28*). The $CD21^{hi}CD27^{+}$ population represents a resting B-cell memory population. These memory cells were detected in blood at steady state and in tissues, with their numbers being transiently boosted by vaccination. Activated

memory $CD21^{lo}CD27^{+}$B-cells can be distinct from ASCs, as they express high levels of CD20. These cells were detectable at steady state in blood and tissues but emerged following vaccination. The fate of each population remains unclear, with both $CD21^{hi}$ and $CD21^{lo}$ cells persisting for at least 4 weeks, but subsiding by one year post-vaccination.

Recent reports described human antigen-specific B-cells with low CD21 expression. A newly-described B-cell phenotype ($CD38^{lo/int}CD20^{hi}CD27^{lo}CD71^{+}$), termed activated B-cells (ABCs), peaks on d14. Based on clonal relationships, ABCs from d7 eventually develop into memory B-cells (*14*). $CD21^{lo}$B-cells ($CD38^{lo}CD21^{lo}CD27^{+}$), which emerge on d14 following IIV, are enriched within influenza-specific B-cells, express transcriptional programs associated with plasma cell differentiation, and are identified as recent emigrants of germinal centers, suggesting they might be precursors of LLPCs (*15*). While we did not measure CD38 expression on rHA^{+}B-cells, a large population of $CD21^{lo}CD27^{+}CD20^{hi}$ influenza-specific B-cells was induced by vaccination and with different dynamics to the ASCs.

Since the initial description of circulating $CXCR5^{+}CD4^{+}$T-cells as counterparts of Tfh cells in blood, their role in regulating vaccine responses is known (*12, 13*). Seminal studies showed that specialization occurs between different cTfh subsets and their ability to stimulate naïve or memory B-cells to differentiate into ASCs (*12, 13*). In that regard, cTfh1 cells have a prominent role in facilitating seroconversion following vaccination, which is predominantly memory-derived (*2, 11*). However, the role of cTfh cells during IIV is limited to the interplay with serum antibodies. We show that activation of cTfh1 cells on d7, correlates with emergence of $CD21^{hi}CD27^{+}$ and $CD21^{lo}CD27^{+}$ influenza-specific B-cells on d14 post-vaccination, implicating cTfh1 cells as key players in the establishment of influenza-specific B-cell memory. Recently, TCR repertoire analysis of cTfh cells following repeated IIV vaccination revealed the recruitment of recurrent clones (*29*), providing evidence that activated cTfh cells are recalled from resting memory pools. Further understanding of the ontogeny, repertoire, specificity and the role of these T-cells during vaccination and infection is key to developing more effective vaccines.

Pre-existing serological memory affected the magnitude of the serological response and individuals who did not seroconvert had higher HAI titres at baseline than seroconverters, consistent with previous observations (*17, 30*). The mechanism is unclear but others suggested that pre-existing antibodies mask or block antigenic epitopes on HA and/or induce the formation of immune complexes, which could aid antigen clearance, thus limiting the B-cell response (*17, 31*). We found an effect of serum titers at baseline on the magnitude

of $CD21^{lo}$ B-cells on d14, although this was only observed for IBV. How exactly pre-existing antibodies limit the vaccine response warrants further research.

Despite the substantial effects of IIV on the B-cell and $CD4^+$/Tfh compartments, other T-cell populations were unaffected. Specifically, IAV- and IBV-specific $CD8^+$ T-cells were unaffected in frequency and phenotype. Whether this is due to antigen content, inadequate inflammation or lack of cross-presentation in the absence of viral replication, is unclear. Given the prominent role of $CD8^+$ T-cells in cross-protective immunity (*4-6*), even against antigenically-shifted strains like avian H5N1(*32*) and H7N9 (*6, 33*), vaccines that establish $CD8^+$ T-cells are of considerable importance.

While vaccination induced robust humoral immunity, the B-cell response was not maintained in peripheral blood over time. This likely reflects the expected contraction of B-cells and their migration to lymphoid tissues. While we cannot infer the relative contribution of contraction and tissue compartmentalization in the observed loss of memory B-cells from blood, nor we know the vaccination and infection history of our donors, our data indicate that memory B-cells are enriched in tissues compared to blood. Accordingly, vaccination in consecutive years induced earlier and larger B-cell responses, despite disappearance of vaccine-induced memory from blood. Similarly, robust memory responses were detected post-vaccination following B-cell depletion by rituximab, implying the presence of memory reservoirs in tissues (*34*). Although our data are derived from unrelated individuals of variable age and exposure history, our study dissects human antigen-specific B-cells across multiple tissues. Our data agree with reports on compartmentalization of human virus-specific (by ELISPOTS) memory B-cells in the spleen (*35*) and distribution of influenza-specific memory B-cells across tissues in mice (*36*). Our analysis suggests that the assessment of long-term vaccine effectiveness in blood may be suboptimal. Notably, our study suggests that vaccine design needs to consider the localization of memory B-cells and the fact that vaccination route affects the B-cell response to vaccination (*37*).

Together, we show that activation of cTfh cells, serological memory and tissue compartmentalization are key factors in human antigen-specific B-cell responses. Our study has implications for the design of effective vaccines against influenza viruses and highlights avenues for further research. Specifically, determining ways to activate cTfh cells and $CD8^+$ T-cells is of utmost importance. It would be pertinent to understand whether and how the limiting effects of pre-existing antibodies on the B-cell response can be overcome. Differential compartmentalization of influenza-specific B-cell subsets across human tissues and the prominent presence of memory B-cells in the lung should be considered with regards

to the vaccination route. Further understating the fate of each B-cell population following vaccination will be fundamental to establishing long-lasting serological and cellular immune memory to influenza viruses.

Materials & Methods

Study design

This study dissected influenza-specific B- and T-cell responses following vaccination with split inactivated influenza viruses and across human tissues. 35 healthy adults (>18 years) were vaccinated over three years (2014-2016). Blood was collected prior to vaccination (d-1) or d0) and on d7, d14 and d28 post-vaccination. Human tissues were used to understand B-cell tissue compartmentalization.

Human blood and tissue samples

Human work was conducted according to the Declaration of Helsinki Principles and the Australian NHMRC Code of Practice. Signed informed consent was obtained from donors or the next of kin. The study was approved by the University of Melbourne Human Ethics Committee (ID1443389.3, ID1443540), Mercy Health Human Research Ethics Committee (IDR14/25) and Australian Red Cross Blood Service (ARCBS) Ethics Committee (ID2015#8).

Spleen, lung and lymph nodes were obtained from deceased organ donors, tonsils from healthy individuals undergoing tonsillectomy (Mater Hospital, North Sydney, NSW, Australia). PBMCs were isolated from buffy packs (ARCBS, West Melbourne, Australia). Cord blood was obtained via the Mercy Women's Hospital (Heidelberg, Australia). Bone marrow mononuclear cells, isolated from the posterior ileac crests of healthy volunteers, were purchased (Lonza, Basel, Switzerland).

Hemagglutination inhibition assay

RDE-treated sera or plasma samples were assessed for antibody titres against the vaccine using standard hemagglutination-inhibition assays. HI titres are reported as the reciprocal of the highest dilution of serum where hemagglutination was completely inhibited.

Whole blood cell surface staining

Numbers were calculated using Trucount tubes and MultiTest (CD3-FITC/CD16+CD56-PE/CD45-PerCP/CD19-APC) (BD Biosciences, San Jose, California, USA).

Ex-vivo live virus stimulation assay

Stimulation with live-virus was performed as described (*6*). At 22 hrs post-infection, cells were harvested and stained with PANEL 2 (table S4). Cells were fixed and permeabilized, along with intracellular antibody staining (BD Cytofix/Cytoperm kit).

PBMC phenotyping

PBMC were stained with MHC-I/peptide tetramers (A2-$M1_{58-66}$, A1-NP_{44-52}, B8-$NP_{225-233}$) conjugated to streptavidin-PE or APC for 1hr at RT. Cells were stained with Panel 3 (table S5), fixed and permeabilized,.

Recombinant HA probes and HA-specific B-cell detection

rHA probes were generated and used for staining HA-specific B-cells as described (*19-21*). PBMCs or tissue samples were stained with panels, listed in tables S6-8 at 4^{o}C for 30mins in 0.1%FCS/PBS. Cells were fixed in 1%PFA for flow cytometry.

Statistical analysis

Significance was assessed using Wilcoxon matched-pairs signed rank test (for changes from baseline), Friedman test (for comparisons between multiple time-points), Mann-Whitney test was used to compare unpaired samples and a paired t-test was used to compare paired tissue samples. Correlations were assessed using Spearman's correlation coefficient (r_s) for non-Gaussian distributions.

Supplementary Materials

Fig S1. Gating strategy for circulating ASCs and activated cTfh1 cells.

Fig S2. Specific activation of cTfh1 cells post-IIV.

Fig S3. Gating strategy for influenza-specific B-cells in PBMC.

Fig S4. Validation of rHA probe staining.

Fig S5. BCR analysis of single rHA^{+}B-cells.

Fig S6. Frequency of IgA^{+} cells in $IgG^{-}D^{-}M^{-}rHA^{+}$B-cells in healthy adults.

Fig S7. Numbers of isotype-specific rHA^{+}(H3N2\Swi) B-cells.

References

1. M. Koutsakos, T.H. Nguyen, W.S. Barclay, K. Kedzierska, Knowns and unknowns of influenza B viruses. *Future Microbiol* **11**, 119-135 (2016).
2. G.M. Li, C. Chiu, J. Wrammert, M. McCausland, S.F. Andrews, N.Y. Zheng, J.H. Lee, M. Huang, X. Qu, S. Edupuganti, M. Mulligan, S.R. Das, J.W. Yewdell, A.K. Mehta, P.C. Wilson, R. Ahmed, Pandemic H1N1 influenza vaccine induces a recall response in humans that favors broadly cross-reactive memory B cells. *Proc Natl Acad Sci U S A* **109**, 9047-9052 (2012).
3. J. Wrammert, D. Koutsonanos, G.M. Li, S. Edupuganti, J. Sui, M. Morrissey, M. McCausland, I. Skountzou, M. Hornig, W.I. Lipkin, A. Mehta, B. Razavi, C. Del Rio, N.Y. Zheng, J.H. Lee, M. Huang, Z. Ali, K. Kaur, S. Andrews, R.R. Amara, Y. Wang, S.R. Das, C.D. O'Donnell, J.W. Yewdell, K. Subbarao, W.A. Marasco, M.J. Mulligan, R. Compans, R. Ahmed, P.C. Wilson, Broadly cross-reactive antibodies dominate the human B cell response against 2009-pandemic H1N1 influenza virus infection. *J Exp Med* **208**, 181-193 (2011).
4. A.J. McMichael, F.M. Gotch, G.R. Noble, P.A. Beare, Cytotoxic T-cell immunity to influenza. *New Eng J Med* **309**, 13-17 (1983).
5. S. Sridhar, S. Begom, A. Bermingham, K. Hoschler, W. Adamson, W. Carman, T. Bean, W. Barclay, J.J. Deeks, A. Lalvani, Cellular immune correlates of protection against symptomatic pandemic influenza. *Nat Med* **19**, 1305-1312 (2013).
6. Z. Wang, Y. Wan, C. Qiu, S. Quinones-Parra, Z. Zhu, L. Loh, D. Tian, Y. Ren, Y. Hu, X. Zhang, P.G. Thomas, M. Inouye, P.C. Doherty, K. Kedzierska, J. Xu,

Recovery from severe H7N9 disease is associated with diverse response mechanisms dominated by CD8(+) T cells. *Nat Commun* **6**, 6833 (2015).
7. C. Chiu, A. H. Ellebedy, J. Wrammert, R. Ahmed, B cell responses to influenza infection and vaccination. *Curr Top Microbiol Immunol* **386**, 381-398 (2015).
8. A. H. Ellebedy, R. Ahmed, Re-engaging cross-reactive memory B cells: the influenza puzzle. *Front Immunol* **3**, 53 (2012).
9. T. Kurosaki, K. Kometani, W. Ise, Memory B cells. *Nat Rev Immunol* **15**, 149-159 (2015).
10. N. Schmitt, S.E. Bentebibel, H. Ueno, Phenotype and functions of memory Tfh cells in human blood. *Trends Immunol* **35**, 436-442 (2014).
11. J. Wrammert, K. Smith, J. Miller, W.A. Langley, K. Kokko, C. Larsen, N.Y. Zheng, I. Mays, L. Garman, C. Helms, J. James, G.M. Air, J.D. Capra, R. Ahmed, P.C. Wilson, Rapid cloning of high-affinity human monoclonal antibodies against influenza virus. *Nature* **453**, 667-671 (2008).
12. R. Morita, N. Schmitt, S.E. Bentebibel, R. Ranganathan, L. Bourdery, G. Zurawski, E. Foucat, M. Dullaers, S. Oh, N. Sabzghabaei, E.M. Lavecchio, M. Punaro, V. Pascual, J. Banchereau, H. Ueno, Human blood CXCR5(+)CD4(+) T cells are counterparts of T follicular cells and contain specific subsets that differentially support antibody secretion. *Immunity* **34**, 108-121 (2011).
13. S.E. Bentebibel, S. Lopez, G. Obermoser, N. Schmitt, C. Mueller, C. Harrod, E. Flano, A. Mejias, R.A. Albrecht, D. Blankenship, H. Xu, V. Pascual, J. Banchereau, A. Garcia-Sastre, A. K. Palucka, O. Ramilo, H. Ueno, Induction of ICOS+CXCR3+CXCR5+ TH cells correlates with antibody responses to influenza vaccination. *Sci Transl Med* **5**, 176ra132 (2013).
14. A.H. Ellebedy, K.J. Jackson, H.T. Kissick, H.I. Nakaya, C.W. Davis, K.M. Roskin, A.K. McElroy, C.M. Oshansky, R. Elbein, S. Thomas, G.M. Lyon, C.F. Spiropoulou, A.K. Mehta, P.G. Thomas, S.D. Boyd, R. Ahmed, Defining antigen-specific plasmablast and memory B cell subsets in human blood after viral infection or vaccination. *Nat Immunol* **17**, 1226-1234 (2016).
15. D. Lau, L.Y.-L. Lan, S.F. Andrews, C. Henry, K.T. Rojas, K.E. Neu, M. Huang, Y. Huang, B. DeKosky, A.-K.E. Palm, G.C. Ippolito, G. Georgiou, P.C. Wilson, Low CD21 expression defines a population of recent germinal center graduates primed for plasma cell differentiation. *Science Immunol* **2**, (2017).
16. S.F. Andrews, Y. Huang, K. Kaur, L.I. Popova, I.Y. Ho, N.T. Pauli, C.J. Henry Dunand, W.M. Taylor, S. Lim, M. Huang, X. Qu, J.H. Lee, M. Salgado-Ferrer, F. Krammer, P. Palese, J. Wrammert, R. Ahmed, P. C. Wilson, Immune history profoundly affects broadly protective B cell responses to influenza. *Sci Transl Med* **7**, 316ra192 (2015).
17. S.F. Andrews, K. Kaur, N.T. Pauli, M. Huang, Y. Huang, P.C. Wilson, High preexisting serological antibody levels correlate with diversification of the influenza vaccine response. *J Virol* **89**, 3308-3317 (2015).
18. Y. Li, J.L. Myers, D.L. Bostick, C.B. Sullivan, J. Madara, S.L. Linderman, Q. Liu, D.M. Carter, J. Wrammert, S. Esposito, N. Principi, J.B. Plotkin, T.M. Ross, R. Ahmed, P.C. Wilson, S.E. Hensley, Immune history shapes specificity of pandemic H1N1 influenza antibody responses. *J Exp Med* **210**, 1493-1500 (2013).
19. A.K. Wheatley, A.B. Kristensen, W.N. Lay, S.J. Kent, HIV-dependent depletion of influenza-specific memory B cells impacts B cell responsiveness to seasonal influenza immunisation. *Sci Rep* **6**, 26478 (2016).
20. A.K. Wheatley, J.R. Whittle, D. Lingwood, M. Kanekiyo, H.M. Yassine, S.S. Ma, S.R. Narpala, M.S. Prabhakaran, R.A. Matus-Nicodemos, R.T. Bailer, G.J. Nabel,

B.S. Graham, J.E. Ledgerwood, R.A. Koup, A.B. McDermott, H5N1 Vaccine-Elicited Memory B cells Are Genetically Constrained by the IGHV Locus in the Recognition of a Neutralizing Epitope in the Hemagglutinin Stem. *J Immunol* **195**, 602-610 (2015).

21. J.R. Whittle, A.K. Wheatley, L. Wu, D. Lingwood, M. Kanekiyo, S.S. Ma, S.R. Narpala, H.M. Yassine, G.M. Frank, J.W. Yewdell, J.E. Ledgerwood, C.J. Wei, A.B. McDermott, B.S. Graham, R.A. Koup, G.J. Nabel, Flow cytometry reveals that H5N1 vaccination elicits cross-reactive stem-directed antibodies from multiple Ig heavy-chain lineages. *J Virol* **88**, 4047-4057 (2014).
22. S.E. Townsend, C.C. Goodnow, R.J. Cornall, Single epitope multiple staining to detect ultralow frequency B cells. *J Immunol Methods* **249**, 137-146 (2001).
23. T. Tiller, E. Meffre, S. Yurasov, M. Tsuiji, M.C. Nussenzweig, H. Wardemann, Efficient generation of monoclonal antibodies from single human B cells by single cell RT-PCR and expression vector cloning. *J Immunol Meth* **329**, 112-124 (2008).
24. J.L. Halliley, S. Kyu, J.J. Kobie, E.E. Walsh, A.R. Falsey, T.D. Randall, J. Treanor, C. Feng, I. Sanz, F.E. Lee, Peak frequencies of circulating human influenza-specific antibody secreting cells correlate with serum antibody response after immunization. *Vaccine* **28**, 3582-3587 (2010).
25. A.E. Hauser, G.F. Debes, S. Arce, G. Cassese, A. Hamann, A. Radbruch, R.A. Manz, Chemotactic responsiveness toward ligands for CXCR3 and CXCR4 is regulated on plasma blasts during the time course of a memory immune response. *J Immunol* **169**, 1277-1282 (2002).
26. N. Wehrli, D.F. Legler, D. Finke, K.M. Toellner, P. Loetscher, M. Baggiolini, I.C. MacLennan, H. Acha-Orbea, Changing responsiveness to chemokines allows medullary plasmablasts to leave lymph nodes. *Eur J Immunol* **31**, 609-616 (2001).
27. M. Odendahl, H. Mei, B.F. Hoyer, A.M. Jacobi, A. Hansen, G. Muehlinghaus, C. Berek, F. Hiepe, R. Manz, A. Radbruch, T. Dorner, Generation of migratory antigen-specific plasma blasts and mobilization of resident plasma cells in a secondary immune response. *Blood* **105**, 1614-1621 (2005).
28. E.J. Kunkel, E.C. Butcher, Plasma-cell homing. *Nat Rev Immunol* **3**, 822-829 (2003).
29. R.S. Herati, A. Muselman, L. Vella, B. Bengsch, K. Parkhouse, D. Del Alcazar, J. Kotzin, S.A. Doyle, P. Tebas, S.E. Hensley, L.F. Su, K.E. Schmader, E.J. Wherry, Successive annual influenza vaccination induces a recurrent oligoclonotypic memory response in circulating T follicular helper cells. *Science Immunol* **2**, (2017).
30. J.S. Tsang, P.L. Schwartzberg, Y. Kotliarov, A. Biancotto, Z. Xie, R.N. Germain, E. Wang, M.J. Olnes, M. Narayanan, H. Golding, S. Moir, H.B. Dickler, S. Perl, F. Cheung, H.C. Baylor, C.H.I. Consortium, Global analyses of human immune variation reveal baseline predictors of postvaccination responses. *Cell* **157**, 499-513 (2014).
31. V.I. Zarnitsyna, J. Lavine, A. Ellebedy, R. Ahmed, R. Antia, Multi-epitope Models Explain How Pre-existing Antibodies Affect the Generation of Broadly Protective Responses to Influenza. *PLoS Pathog* **12**, e1005692 (2016).
32. L.Y. Lee, L.A. Ha do, C. Simmons, M.D. de Jong, N.V. Chau, R. Schumacher, Y.C. Peng, A. J. McMichael, J. J. Farrar, G. L. Smith, A. R. Townsend, B. A. Askonas, S. Rowland-Jones, T. Dong, Memory T cells established by seasonal human influenza A infection cross-react with avian influenza A (H5N1) in healthy individuals. *J Clin Invest* **118**, 3478-3490 (2008).
33. C.E. van de Sandt, J.H. Kreijtz, G. de Mutsert, M.M. Geelhoed-Mieras, M.L. Hillaire, S.E. Vogelzang-van Trierum, A. D. Osterhaus, R. A. Fouchier, G. F. Rimmelzwaan,

Human cytotoxic T lymphocytes directed to seasonal influenza A viruses cross-react with the newly emerging H7N9 virus. *J Virol* **88**, 1684-1693 (2014).
34. A. Cho, B. Bradley, R. Kauffman, L. Priyamvada, Y. Kovalenkov, R. Feldman, J. Wrammert, Robust memory responses against influenza vaccination in pemphigus patients previously treated with rituximab. *JCI Insight* **2**, (2017).
35. M. Mamani-Matsuda, A. Cosma, S. Weller, A. Faili, C. Staib, L. Garcon, O. Hermine, O. Beyne-Rauzy, C. Fieschi, J.O. Pers, N. Arakelyan, B. Varet, A. Sauvanet, A. Berger, F. Paye, J. M. Andrieu, M. Michel, B. Godeau, P. Buffet, C.A. Reynaud, J.C. Weill, The human spleen is a major reservoir for long-lived vaccinia virus-specific memory B cells. *Blood* **111**, 4653-4659 (2008).
36. H.M. Joo, Y. He, M.Y. Sangster, Broad dispersion and lung localization of virus-specific memory B cells induced by influenza pneumonia. *Proc Natl Acad Sci USA* **105**, 3485-3490 (2008).
37. H.M. Joo, Y. He, A. Sundararajan, L. Huan, M.Y. Sangster, Quantitative analysis of influenza virus-specific B cell memory generated by different routes of inactivated virus vaccination. *Vaccine* **28**, 2186-2194 (2010).

Acknowledgements: We thank study participants, organ donors, coordinators of DonateLife-Victoria for obtaining organ tissues, Lina Mariana and Cameron Kos for their assistance. We thank Nicola Bird, Katherine Watson, Maria Auladell Bernat, Louise Carolan, Malet Aban, Thakshila Amarasena, Sheilajen Alcantara for their technical assistance. We are grateful to and Drs Ali Ellebedy,. Rafi Ahmed and. Carola Vinuesa for providing their expertise.

Funding: This work was supported by NHMRC Program Grant ID1071916 (KK) and ID1052979 (SJK), NHMRC project grants ID1129099 (AKW) and ID1125164 (AWC). MK and SN are supported by a Melbourne International Research Scholarship (MIRS) and Melbourne International Fee Remission Scholarship (MIFRS), EBC is an NHMRC Peter Doherty Fellow, SS is supported by the Victoria-India Doctoral Scholarship (VIDS) and MIFRS. WHO Collaborating Centre for Reference Research on Influenza is supported by the Australian Government Department of Health. SIM is supported by JDRF Career Development Award (5-CDA-2014-210-A-N), NHMRC (ID1123586). SR is an employee of Seqirus Ltd. SGT is supported by NHMRC Program and project grants. SGT, SJK and KK are NHMRC Research Fellows.

Author contributions: M.K., T.H.O.N., K.K. designed experiments. M.K., A.K.W. A.F., T.H.O.N. performed experiments. M.K., L.L., E.B.C., S.S., S.N., T.H.O.N. processed blood and tissues. K.L.L., A.C.H. performed serological analysis. M.L., T.L., S.I.M., G.P.W., L.M.W., S.G.T. obtained and provided tissues. A.K.W., S.J. K. generated rHA probes. M.K.,

A.W.C., T.H.O.N., K.K. analyzed data. M.K., T.H.O.N., K.K. wrote the manuscript. All authors revised the manuscript.

Competing interests: The author, Steven Rockman, holds shares in CSL Ltd which is the parent company to Seqirus which is the manufacturer of Influenza vaccines (Afluria, Agripal, Flucelvax, FluAd). The other authors declare no competing interests.

Figure legends

Figure 1. Vaccination induces activation of cTfh cells and transient ASCs. (A) Study design and vaccine composition. (B) Representative FACS plots and (C) numbers of $ICOS^+PD\text{-}1^+$cTfh1 cells post-vaccination (n=42). (D) CD38 upregulation on activated cTfh1 cells. (E) Frequency of $CD38^{hi}$ cells in the $ICOS^+PD\text{-}1^+$cTfh1 population (n=26, 2016-cohort). (F) Representative FACS plots and (G) numbers of $CD27^{hi}CD38^{hi}$ASCs post-vaccination (n=42). (H) Expression of CXCR3 and (I) frequency of $CXCR3^+$ASCs post-vaccination. (J-K) MFI of CXCR3 (J) and CXCR5 (K) expression on ASCs and non-ASCs at d7 (n=26, 2016 cohort). (L) Serological response to vaccination, measured as fold-change in HAI titres (2014: n=7, 2015: n=16, 2016: n=26). Bars/lines indicate the median. Statistical significance from baseline or between groups was determined using Wilcoxon matched-pairs signed rank test (**P<0.005, ***P<0.001. ****P<0.0001).

Figure 2. Influenza A- and B-specific B-cell pools differ in size and isotype distribution in peripheral blood. PBMCs were stained with rHA probes from the H1, H3 and B viruses to detect influenza-specific IgD^-B-cells. (A) Representative FACS plots. (B) Absolute numbers of rHA^+IgD^- B-cells/ml of blood. (C) Isotype distributions for rHA^+ B-cell populations. Representative FACS plots of IgG^+ versus IgM^+ B-cells. (D) Pie charts indicate median frequency (n=42). (E-G) Numbers of (E) IgG^+B-cells, (F) IgA^+B-cells, (G) IgM^+B-cells of rHA^+ populations. (H-I) CD27/CD21 phenotype of rHA^+ populations. (H) Representative FACS plots. (I) Isotype distributions of rHA^+B-cells. (J) Numbers of $CD21^+CD27^+$B-cells/ml blood. Bars/lines indicate the median (n=42). Significance between viruses was determined using Wilcoxon matched-pairs signed-rank test. *P<0.05, **P<0.005, ***P<0.001 and ****P<0.0001.

Figure 3. IIV induces $CD21^{hi}CD27^+$ and $CD21^{lo}CD27^+$ influenza-specific B-cells. (A) Numbers of rHA^+IgD^-B-cells before and post-vaccination. (A) Representative FACS plots of

rHA$^+$B-cells post-vaccination. (B) Numbers of rHA$^+$B-cells/ml blood for each vaccine component. (C) Representative FACS plots and (D) frequency of CD27$^+$CD20$^-$rHA$^+$B-cells before and post-vaccination. (E) Numbers of isotype-specific rHA$^+$B-cells. (F) Representative FACS plots for d0 and d14; (G) Numbers of CD21^{hi}CD27$^+$ and CD21^{lo}CD27$^+$ IgG$^+$rHA$^+$B-cells. (E,G) Pooled data from 2015 and 2016 cohorts, n=42. Bars indicate the median. Statistical significance for changes from baseline was determined using Wilcoxon matched-pairs signed rank test (*P<0.05, **P<0.005, ***P<0.001, ****P<0.0001).

Figure 4. Circulating Tfh cells correlate with a boosting of influenza-specific memory B-cells. (A) Correlation between d7 ASCs and fold-change in serum titers post-vaccination. (B) Numbers of ASC on d7 in seroconverters (S) (n=19) and non-seroconverters (NS) (n=7). (C) Fold-change on d28 over baseline in HAI serum titres from pooled data, from three vaccine components of the 2014-cohort, at different time-points. (D) Correlation between d7 ICOS$^+$PD-1$^+$cTfh1 cells and fold-change in serum titers post-vaccination. (E) Numbers of ICOS$^+$PD-1$^+$cTfh1 cells on d7 in seroconverters and non-seroconverters. (F) Correlation between d7 ASCs and ICOS$^+$PD-1$^+$cTfh1 cells. (G) Correlation between fold-changes in CD21^{hi}CD27$^+$B-cells or CD21^{lo}CD27$^+$B-cells on d14 and numbers of ICOS$^+$PD-1$^+$cTfh1 on d7. (A, D, F) Data from 2015 and 2016 cohorts (n=42). (G) Data from 2015-cohort (n=16). (A, D, F, G-I) Correlation was assessed using Spearman's correlation coefficient (r_s). (B, E) Bars indicate the median. Statistical significance was determined using the Mann-Whitney test (*P<0.05).

Figure 5. Pre-existing antibodies negatively correlate with the serological response and the magnitude of the CD21^{lo}B-cell response. (A) HAI titers at baseline in seroconverters (S) and non-seroconverters (NS). Seroconversion was defined as a change in HAI titer ≥4. Dotted line indicates a HAI of 40. Bars indicate the geometric mean. Statistical significance was determined using the Mann-Whitney test (**P<0.005). (B) Correlation between HAI titres at baseline and fold-change in serum titers post-vaccination. Correlations between total HAI titres at baseline and (C) total fold-change in serum titers (d28/d0), (D) numbers of ASCs or (E) ICOS$^+$PD-1$^+$cTfh1 cells on d7. Correlation between total HAI titres at baseline and the fold-change in (F) CD21^{hi}CD27$^+$ or (G) CD21^{lo}CD27$^+$ IgG$^+$B-cells on d14. Correlation was assessed using Spearman's correlation coefficient (r_s).

Figure 6. Vaccination fails to induce CD8$^+$ and innate T-cell responses. (A-B) IFNγ/TNF production following stimulation with IAV-H1N1 or IBV-B/Phuket. (A) Representative FACS plots of H1N1 stimulation. (B) Numbers of IFNγ$^+$ cells/ml blood after IAV or IBV stimulation (n=7, 2015 cohort). 'No virus' controls was subtracted. Significance for changes between time-points was determined using the Friedman test. (C) IAV-specific CD8$^+$ T-cells were detected by peptide/MHC-I tetramers. FACS plots are gated on CD3$^+$cells and percentages are based on CD8$^+$T-cells. (D) Longitudinal tracking of % tetramer$^+$CD8$^+$T-cells (n=3). Arrows indicate vaccination. (E) FACS plots of CD27/CD45RA expression on tetramer$^+$CD8$^+$T-cells, (F) Longitudinal tracking of activated CD27$^+$CD45RA$^-$tetramer$^+$ CD8$^+$T-cells (n=3). (G) T-cell subsets were assessed for activation and differentiation markers. Bars indicate the median. Data are from randomly selected donors (n=14, 2014-2015 cohorts).

Figure 7. Vaccine-induced influenza-specific B-cells are not maintained in peripheral blood. Responses in (A) antibody serum titers, (B) numbers of IgD$^-$rHA$^+$B-cells, (C) pie graphs of isotype distribution of each rHA$^+$ population, (D) changes in isotype-specific rHA$^+$B-cells and (E) numbers of CD21^{hi} and CD21^{lo} influenza-specific B-cells at baseline, d28 and >d350 (n=9 from 2015-cohort). Significance for changes from baseline was determined using Wilcoxon matched-pairs signed rank test (*P<0.05, **P<0.005). (F-H) Numbers of (F) total IgD$^-$rHA$^+$B-cells and (G) CD21^{hi} and (H) CD21^{lo}IgG$^+$rHA$^+$B-cells in individuals vaccinated in 2015 and 2016.

Figure 8. Influenza-specific B-cells show distinct patterns of tissue compartmentalization. (A) Frequency of CD19$^+$CD10$^-$B-cells across tissues. (B) CD21/CD27 phenotype and (C) isotype of B-cells across tissues. (D) Frequency of rHA$^+$ (H1/H3) IgD$^-$B-cells across tissues. Representative FACS plots are shown. (E) Phenotype distribution and (F) isotype distribution of rHA$^+$B-cells across tissues. (A and D) Bars indicate median. (B, C, E, F) Lines indicate mean and error bars show SEM. Adult blood: n=5, cord blood: n=5, bone marrow: n=5, tonsil: n=5, lymph node: n=3, lung: n=3, spleen: n=7. (H) PBMCs from paired blood and spleen samples were analyzed. Frequency of each CD21/CD27 population within total B-cells for each blood and spleen pair (n=5) is shown. Significance was assessed using a paired t-test (*P<0.05, **P<0.005).

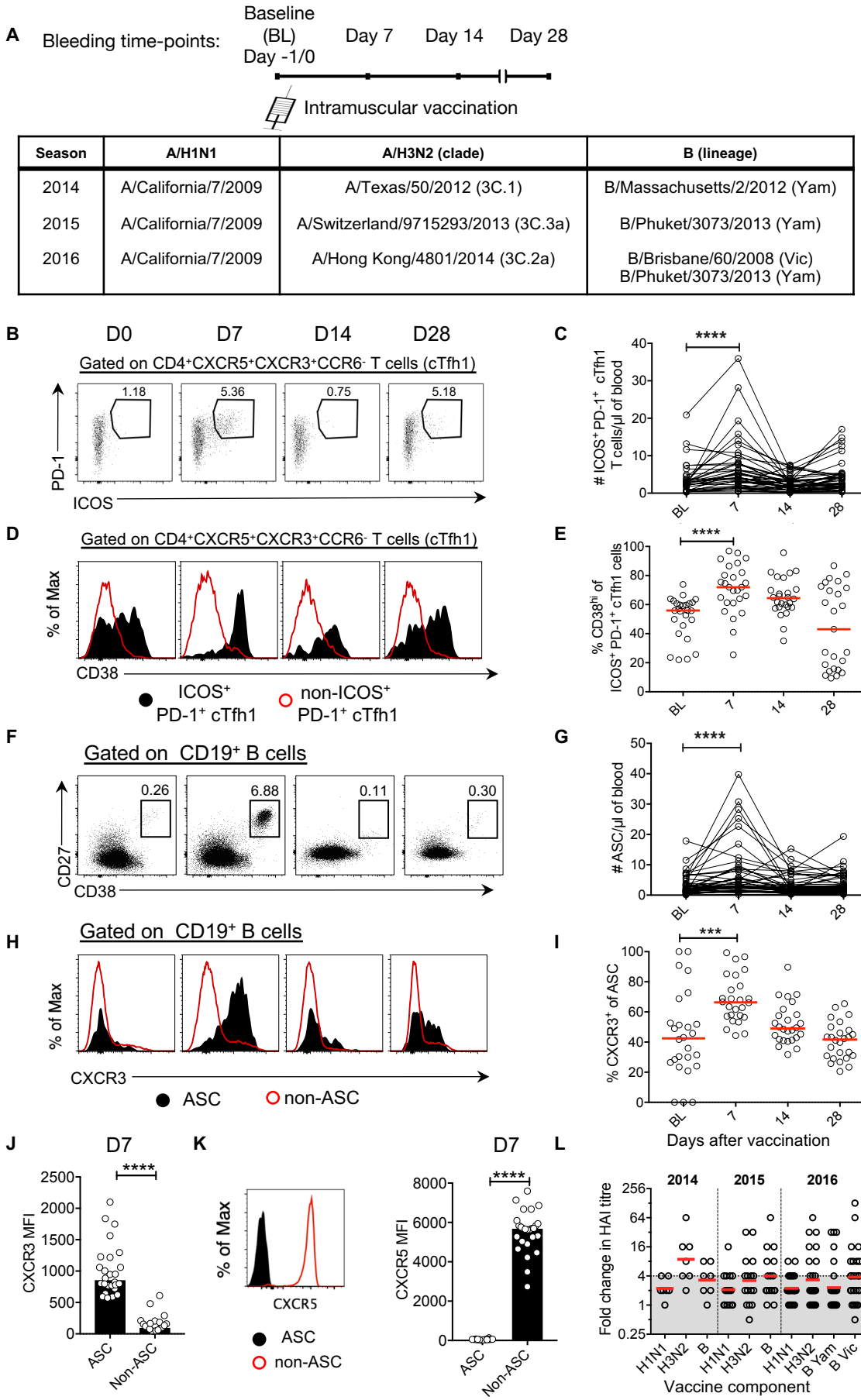

Season	A/H1N1	A/H3N2 (clade)	B (lineage)
2014	A/California/7/2009	A/Texas/50/2012 (3C.1)	B/Massachusetts/2/2012 (Yam)
2015	A/California/7/2009	A/Switzerland/9715293/2013 (3C.3a)	B/Phuket/3073/2013 (Yam)
2016	A/California/7/2009	A/Hong Kong/4801/2014 (3C.2a)	B/Brisbane/60/2008 (Vic) B/Phuket/3073/2013 (Yam)

Koutsakos *et al*, Fig. 1

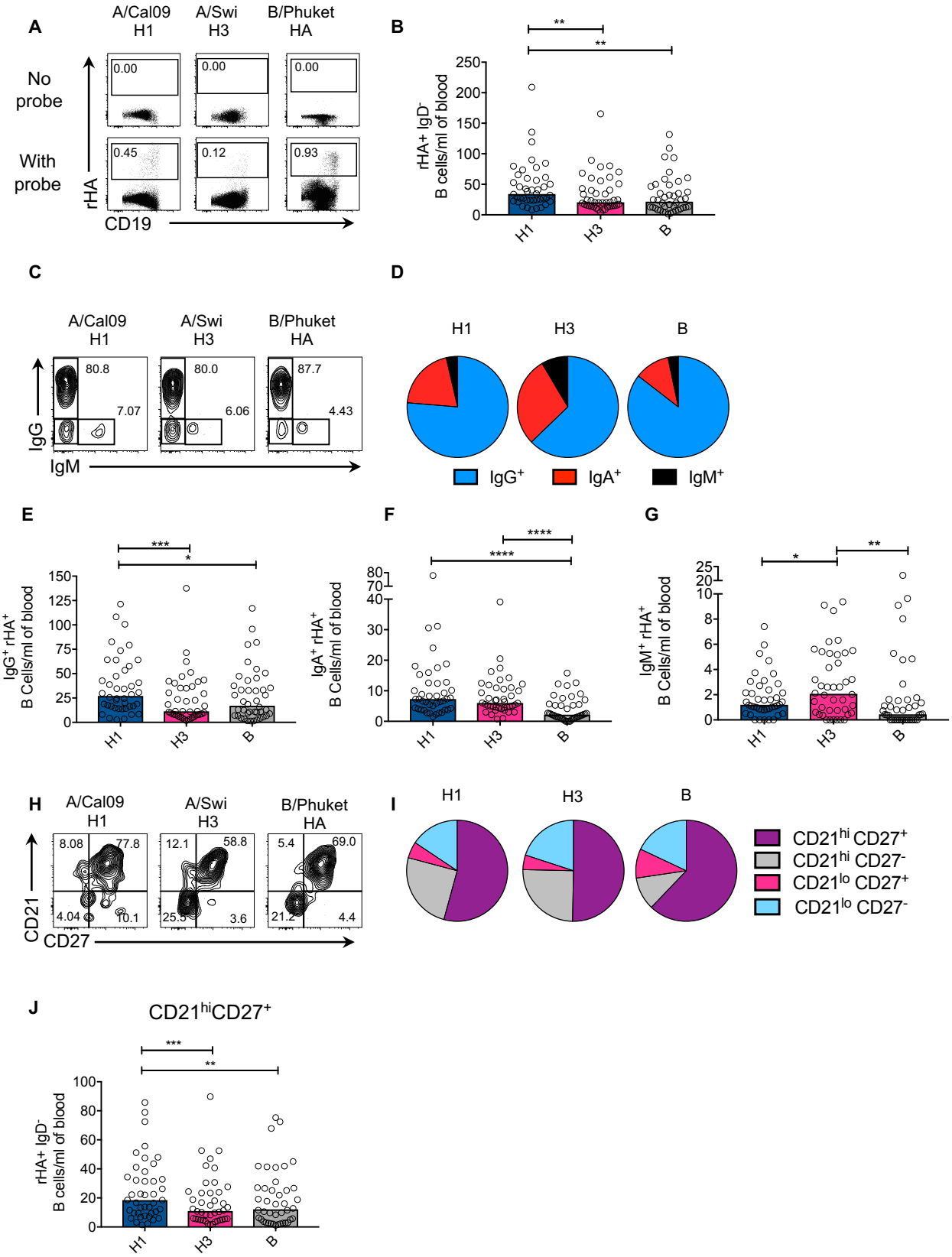

Koutsakos *et al*, Fig. 2

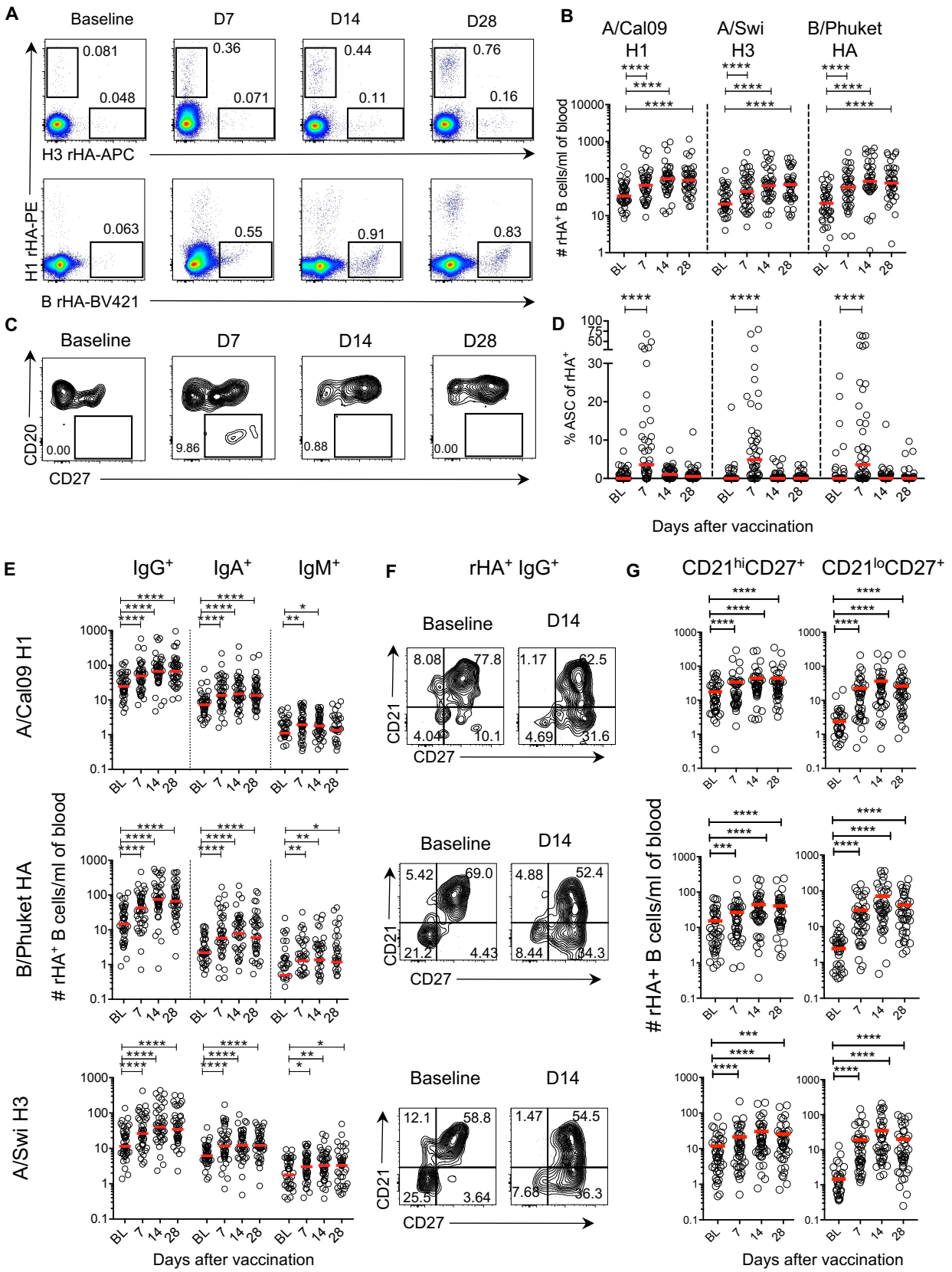

Koutsakos *et al*, Fig. 3

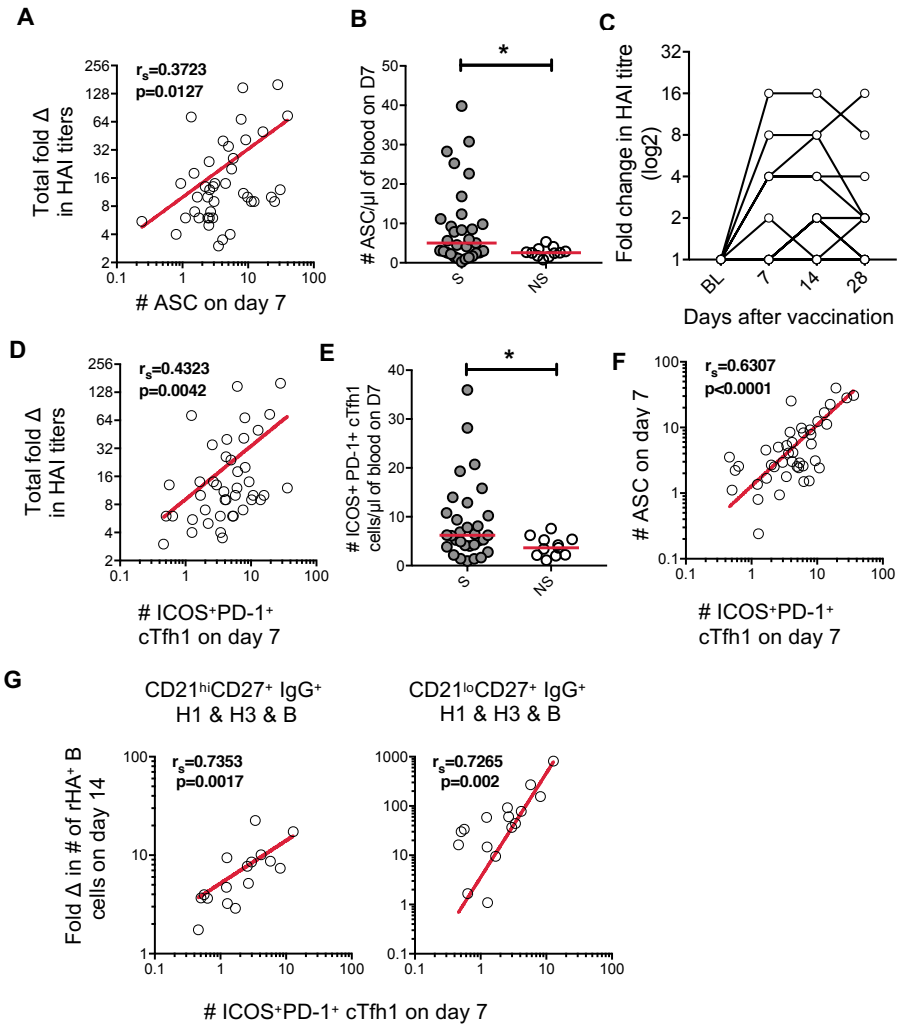

Koutsakos *et al*, Fig. 4

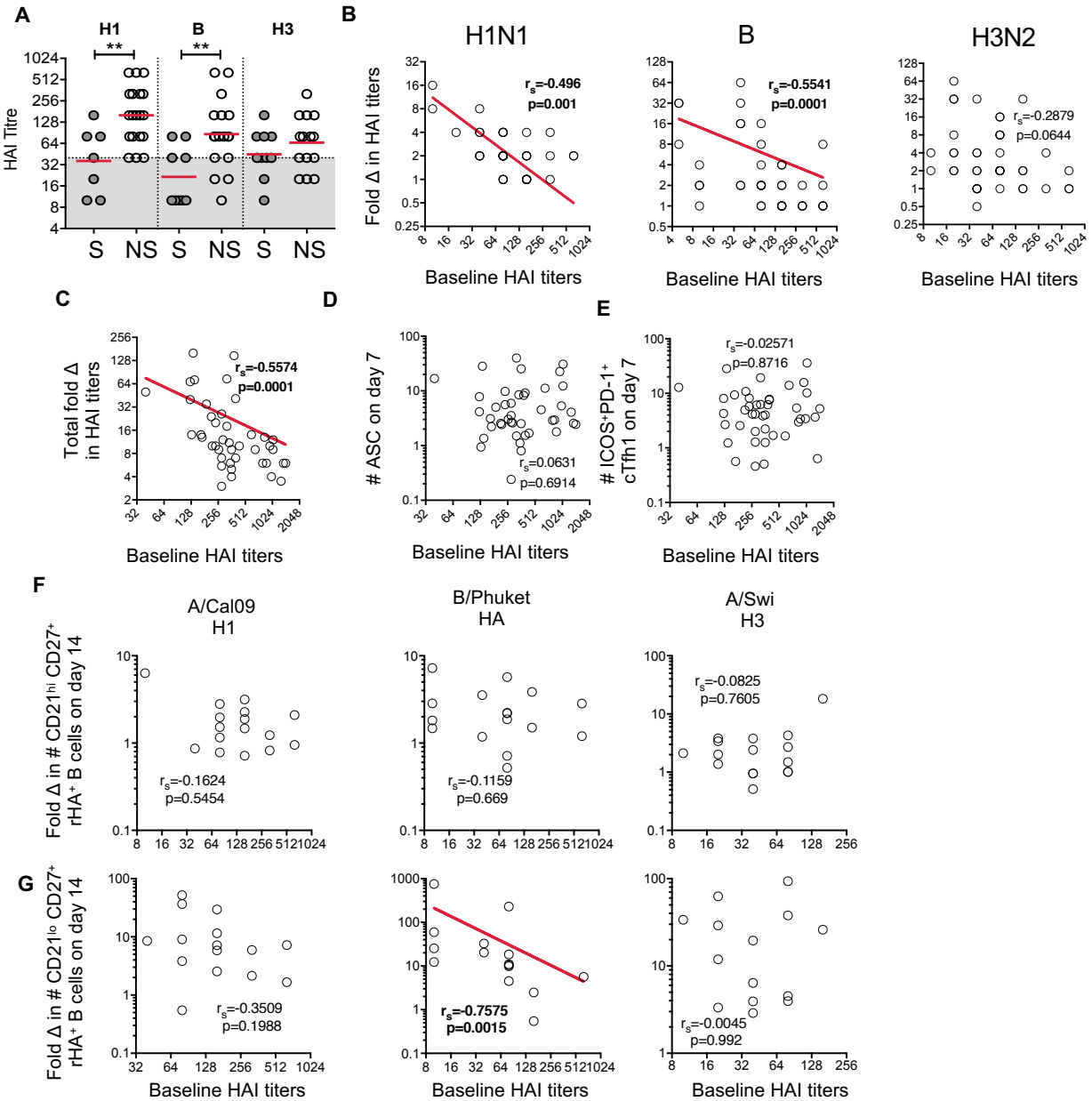

Koutsakos *et al*, Fig. 5

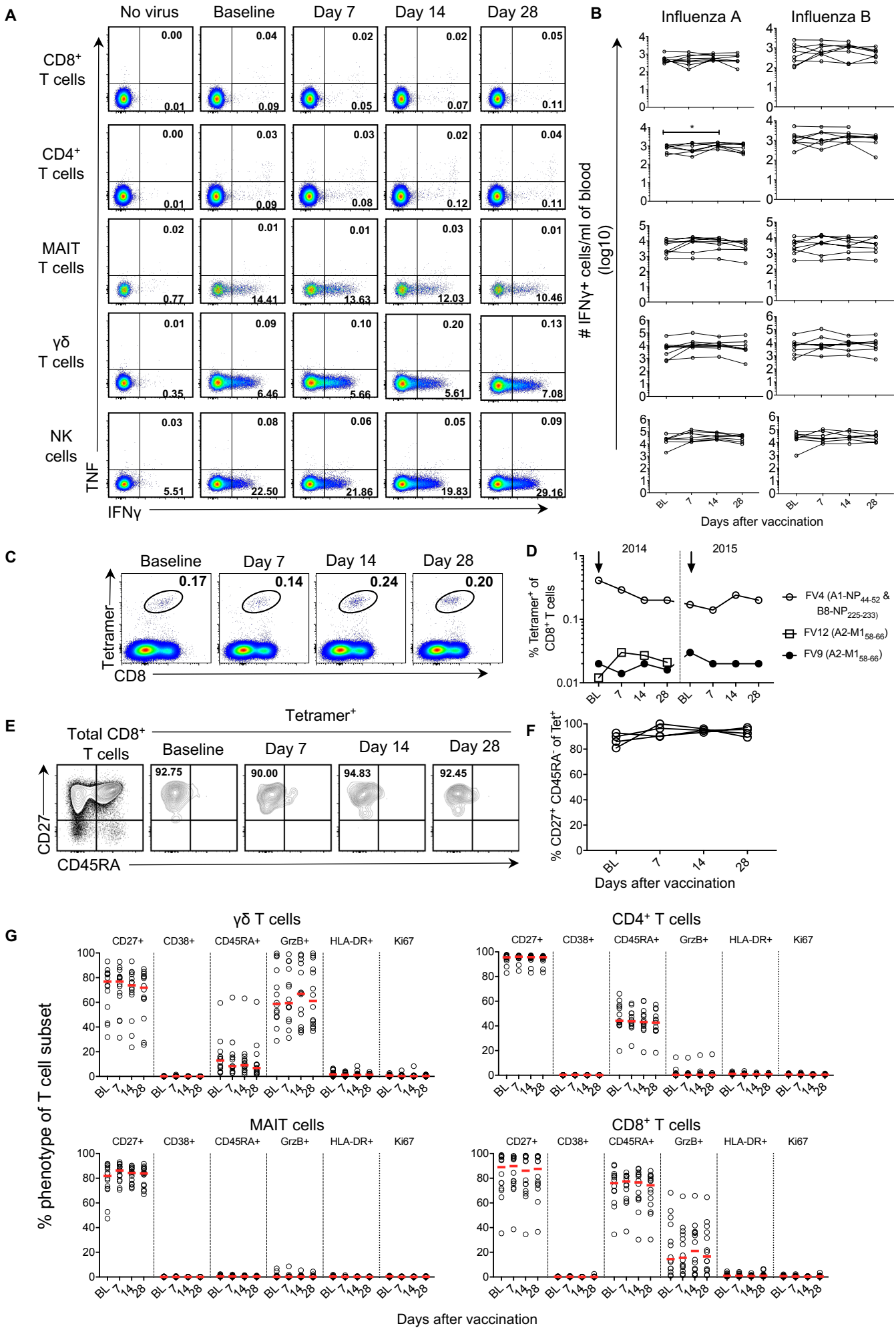

Koutsakos *et al*, Fig. 6

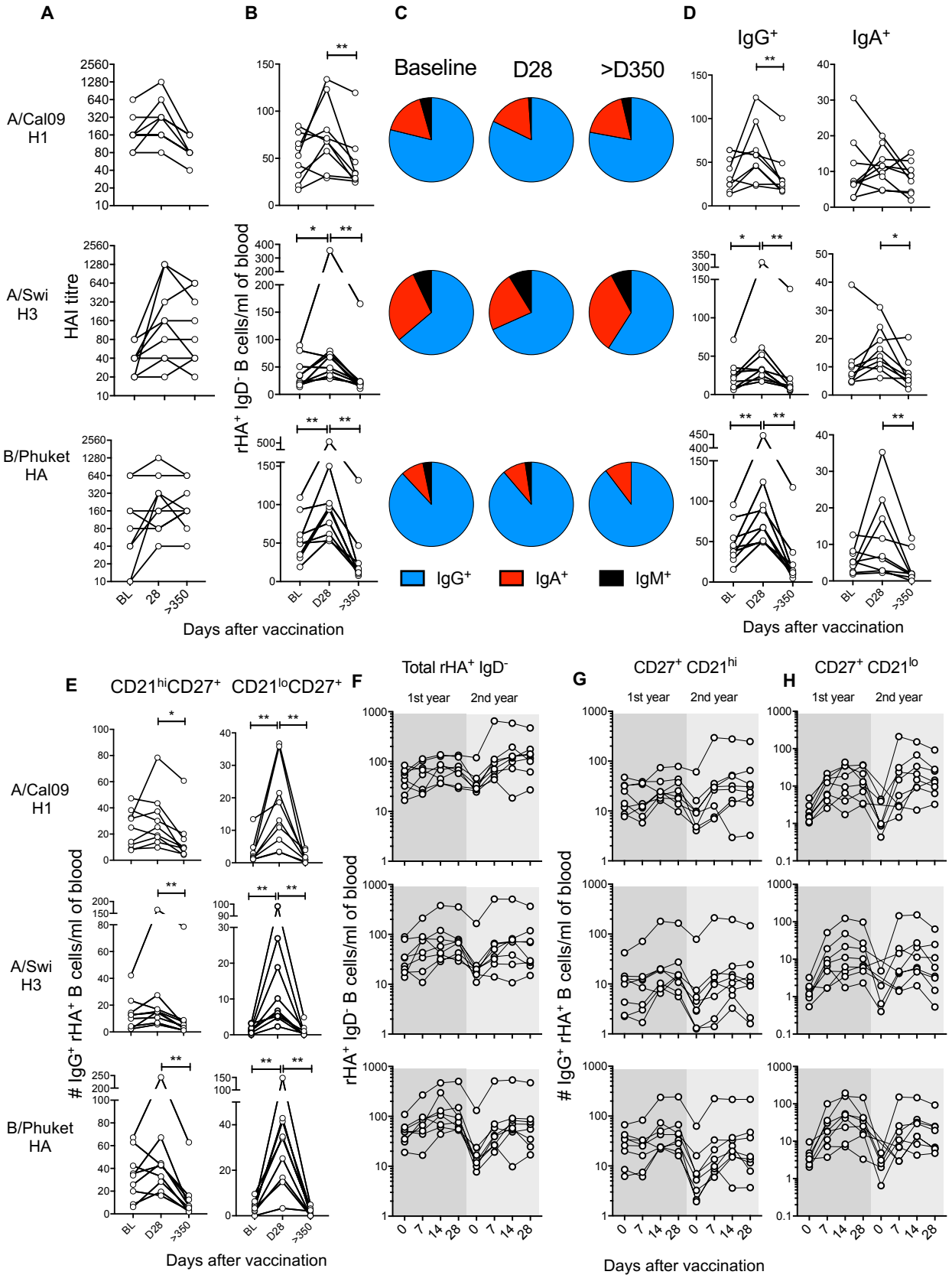

Koutsakos *et al*, Fig. 7

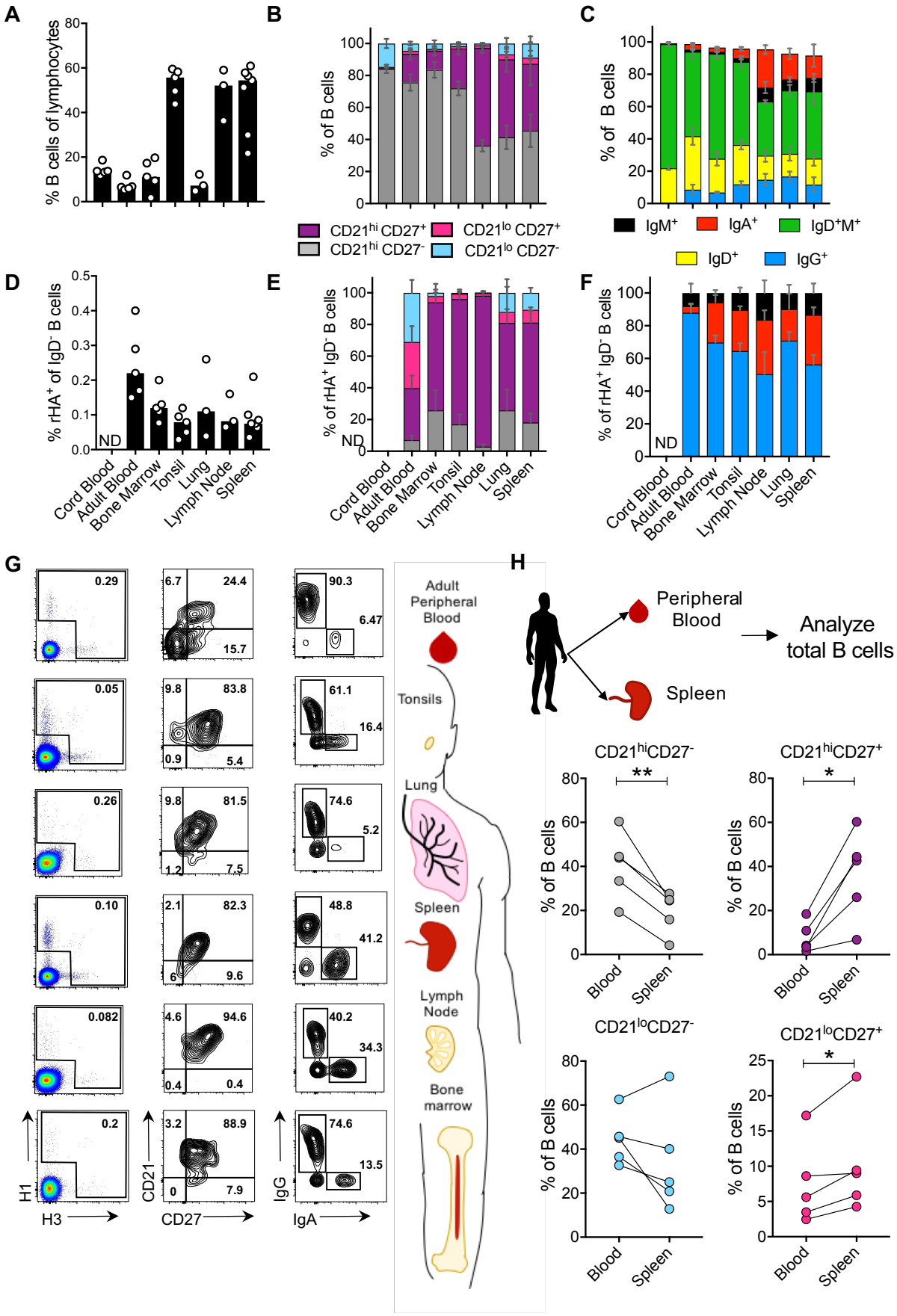

Koutsakos *et al*, Fig. 8

Materials & Methods

Study design

This study aimed to dissect the influenza-specific B and T cell responses following vaccination with split inactivated influenza viruses and across human tissues. To that end, 35 healthy adults (>18 years old) were vaccinated over three years (2014-2016) with the trivalent influenza vaccine (TIV) (2014, n=7 and 2015, n=16) or the 2016 quadrivalent influenza vaccine (QIV) (2016, n=26), with selected individuals participating in consecutive years (table S1). Peripheral blood samples were collected in heparinized tubes prior to vaccination (day -1 or 0) and on days 7, 14 and 28 following vaccination. For individuals participating in both 2015 and 2016 years, the 2016 baseline sample was used as the 1-year time-point (>350 days). Influenza-specific B cells were identified using recombinant hemagglutinin probes and flow cytometry. ASCs and serum antibody titres were assessed in all three cohorts. Circulating Tfh and influenza-specific B cells were assessed in the 2015 and 2016 cohorts. Cellular immunity was assessed in selected donors from the 2014 and 2015 cohort. One donor in the 2016 cohort reported feeling unwell with symptoms of unrelated sickness and those samples were excluded from analysis. In cases where less than the total number of donors were analysed, donors were randomly selected for analysis. No other blinding or randomization protocols were applied and no outliers were excluded.

Human blood and tissue samples

Human experimental work was conducted according to the Declaration of Helsinki Principles and according to the Australian National Health and Medical Research Council Code of Practice. Signed informed consent was obtained from all blood and tissue donors prior to the study. Tissues from deceased organ donors were obtained following written informed consent from the next of kin. The study was approved by the University of Melbourne Human Ethics Committee (ID 1443389.3 and 1443540), the Mercy Health Human Research Ethics Committee (ID R14/25) and the Australian Red Cross Blood Service (ARCBS) Ethics Committee (ID 2015#8).

Spleen, lung and lymph node samples were obtained from deceased organ donors. Spleen and lymph node samples were obtained via DonateLife Victoria (table S2). Lung samples were obtained via the Alfred Hospital's Lung Tissue Biobank. Tonsils were obtained from healthy individuals undergoing tonsillectomy (Mater Hospital, North Sydney, NSW,

Australia). PBMCs were isolated from buffy packs obtained from the ARCBS (West Melbourne, Australia). Umbilical cord blood was obtained via the Mercy Women's Hospital (Heidelberg, Australia). Bone marrow mononuclear cells, isolated from the posterior ileac crests of healthy volunteers, were commercially purchased (Lonza, Basel, Switzerland).

Processing of peripheral blood and human tissues

PBMC were isolated by Ficoll-Paque (GE Healthcare, Uppsala, Sweden) density-gradient centrifugation and cryopreserved. Mononuclear cells were isolated and cryopreserved from spleen, lymph nodes and lungs by mechanical dissociation, followed by enzymatic digestion with 1mg/ml of Type III Collagenase (Worthington Biochemical Corporation, Lakewood, New Jersey, US) in RPMI for 1 hour at 37^{o}C. Cells were forced through a 70μm strainer and red blood cells were lysed using a lysis solution containing 0.168M ammonium chloride, 0.01mM EDTA and 12mM sodium bicarbonate in ddH_2O. Tonsil mononuclear cells were further isolated by density-gradient centrifugation after lysing the red blood cells. HLA class I molecular typing was performed by the Victorian Transplantation and Immunogenetics Service (ARCBS, West Melbourne, Victoria, Australia) using the Luminex platform and microsphere technology (One Lambda, Canoga Park, CA, USA), with LABType SSO HLA typing kits (One Lambda).

Viruses

Influenza A (A/California/7/2009 H1N1pdm09) and B (B/Phuket/3073/2013) viruses were grown in 10-day old embryonated chicken eggs at 33^{o}C for 72 hours. Allantoic fluid was harvested and titrated using standard plaque assays in MDCK cells.

Hemagglutination inhibition assay

RDE-treated sera or plasma samples were assessed for antibody titres against the vaccine components using standard hemagglutination inhibition assays with 1% turkey red blood cells (H1N1 and IBV) or 1% guinea pig red blood cells in the presence of oseltamivir (H3N2). Briefly, following serial dilutions in PBS (1:10 to 1:1280), samples were incubated with the relevant influenza viruses. HI titres are reported as the reciprocal of the highest dilution of serum where hemagglutination was completely inhibited.

Whole blood cell surface staining

Absolute cell numbers were calculated using BD Trucount tubes and BD MultiTest (CD3 FITC/CD16+CD56 PE/CD45 PerCP/CD19 APC) according to manufacturer's instructions (BD Biosciences, San Jose, California, USA). Fresh whole blood (200ul) was stained with PANEL 1 (table S3) for 20 mins at room temperature (RT) in the dark. Samples were then lysed with BD FACS Lysing solution, washed and fixed with 1% PFA. All samples for flow cytometry were acquired using an LSR Fortessa (BD Biosciences). All flow cytometry data were analysed using FlowJo 10.

Ex-vivo live virus stimulation assay

Stimulation with live virus was performed as described (*8*). Briefly, $1.5x10^6$ PBMC were thawed, washed twice in serum-free media and then infected with influenza A or B (A/Cal09 H1N1pdm09, B/Phuket) for 1 hr at 37^{o}C at a multiplicity of infection (MOI) of 4. Following the 1 hr inoculation, cells were washed once in RPMI+10% fetal calf serum and incubated at 37^{o}C for 3 hrs. Brefeldin A (BD GolgiPlugTM) was then added and cells were incubated for another 18 hrs. After a total of 22 hrs post-infection, cells were harvested and stained with PANEL 2 (table S4). Cells were fixed and then permeabilized, along with intracellular antibody staining, using the BD Cytofix/Cytoperm kit according to manufacturer's instructions.

Phenotyping of PBMC

PBMC were thawed and washed twice in serum-free media then stained with MHC-I/peptide tetramers (A2-$M1_{58-66}$ or A1-NP_{44-52} and B8-$NP_{225-233}$) conjugated to either streptavidin-PE or APC for 1 hr at RT in the dark. Cells were then stained with Panel 3 (table S5), fixed then permeabilized, as above.

Recombinant HA probes and HA-specific B cell detection

Recombinant (r) HA probes were generated and used for staining HA-specific B cells as described (*25-27*). rHA probes contained mutations (Y98F for influenza A and T190G for influenza B), which prevent binding to sialic acids, thereby reducing non-specific binding, as previously described (*27*). Thawed PBMCs were stained with PANEL 4a (2014 and 2015 samples) and PANEL4b (2016 samples) (tables S6 and S7), while human tissue samples were stained with PANEL 4c (table S8). Staining with rHA probes was performed at the same time

as cell surface staining at 4°C for 30 mins in 0.1% FCS/PBS. Cells were then fixed in 1% PFA for flow cytometry.

Validation of rHA-specific B cell probes.

Dual rHA probe staining was performed with two rHA-probes of the same specificity, but conjugated to different fluorochromes (PE and APC). Blocking of rHA staining with sheep anti-HA sera (kindly provided by the Seqirus vaccine facility) was performed by using sheep anti-sera from animals immunized with either A/Singapore/GP1908/2015 (IVR-180), H3N2: A/Hong Kong/4801/2014-like or B/Wisconsin/1/2010-like antigens to block cognate rHA probe binding. rHA probes (H1/Cal09-PE, H3/Swi-APC, B/PHU-BV421) were mixed and incubated with H1, H3 or B anti-sera or PBS for 30 mins at room temperature. PBMCs were then stained with pre-incubated rHA probes, as described above.

BCR sequencing of rHA-specific B cells were performed by single-cell FACS-sorting of $CD19^+$ IgD^- IgM^- IgG^+ $CD27^+$ rHA^+ B cells directly *ex vivo* from PBMC samples. The BCR sequences were recovered using a multiplex PCR approach (*29*).

B cell ELIPOTS were set up using PBMCs from day 0 or day 14 vaccinees. PBMCs were cultured in the presence of sCD40L (10µg/ml) (Enzo), IL-21 (50ng/ml) (eBioscience) and CpG (ODN 2006-G5, 5µg/ml) (InvivoGen) for 5 days and then assayed by ELISPOT for 14 hours on plates coated with cognate inactivated virus preparations and stained with a goat anti-human IgG detection antibody conjugated on alkaline phosphatase (Jackson Immunoresearch).

Statistical analysis

All statistical analyses were performed using Prism (GraphPad, source). Significance was assessed using Wilcoxon matched-pairs signed rank test (for changes from baseline), Friedman test (for comparisons between multiple time-points), the Mann-Whitney test was used to compare unpaired samples and a paired t-test was used to compare paired tissue samples as indicated in figure legends. P values lower than 0.05 were considered statistically significant with *$p<0.05$,**$p<0.005$, ***$p<0.001$ and ****$p<0.0001$. Correlations were assessed using Spearman's correlation coefficient (r_s) for non-Gaussian distributions.

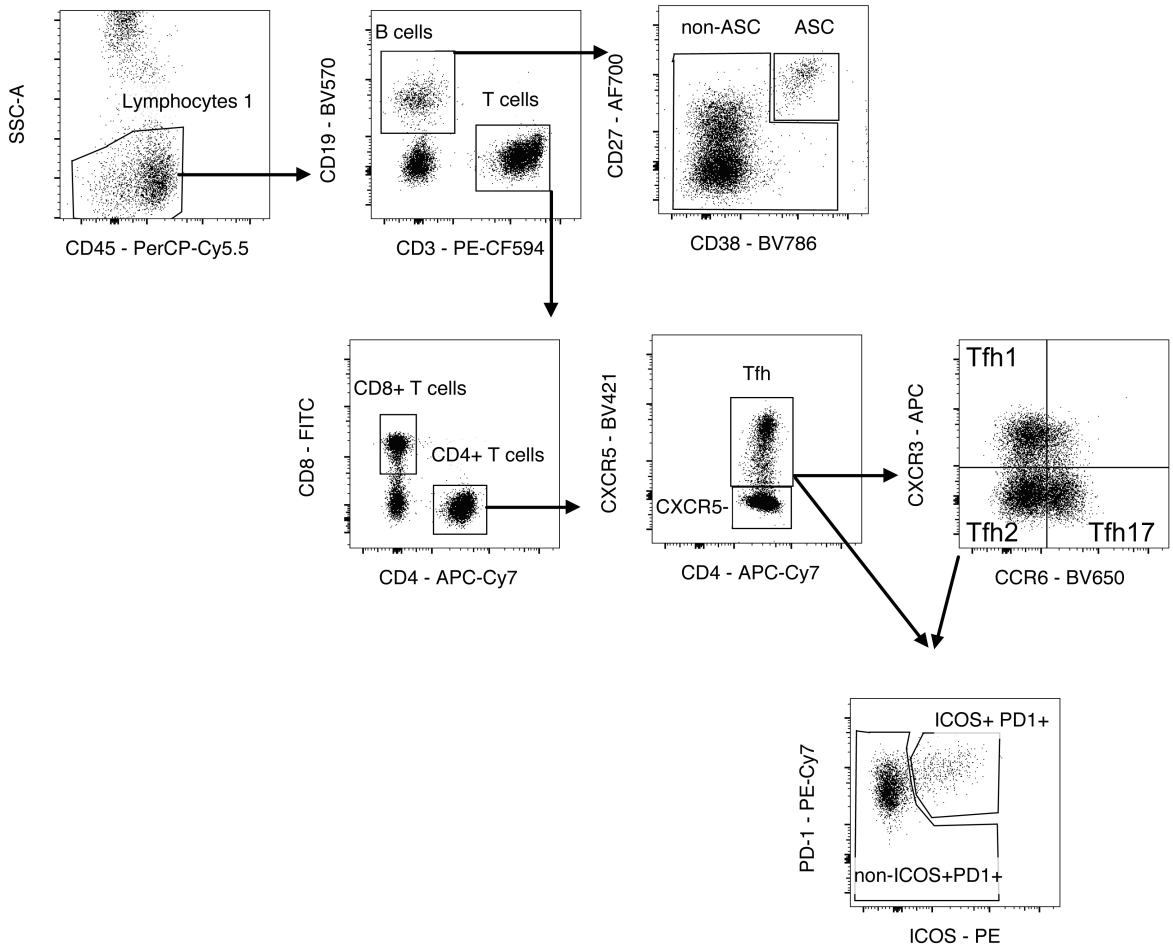

Fig S1. Gating strategy for circulating ASCs and activated cTfh1 cells. T cells and B cells were gated as $CD3^+$ and $CD19^+$ respectively from $CD45^+$ lymphocytes. ASCs ($CD38^{hi}CD27^+$) were identified within B cells. Tfh cells were identified within $CD4^+$ T cells and further divided into three subsets based on CXCR3 and CCR6. ICOS and PD-1 expression were used to identify activated Tfh cells ($ICOS^+PD\text{-}1^+$).

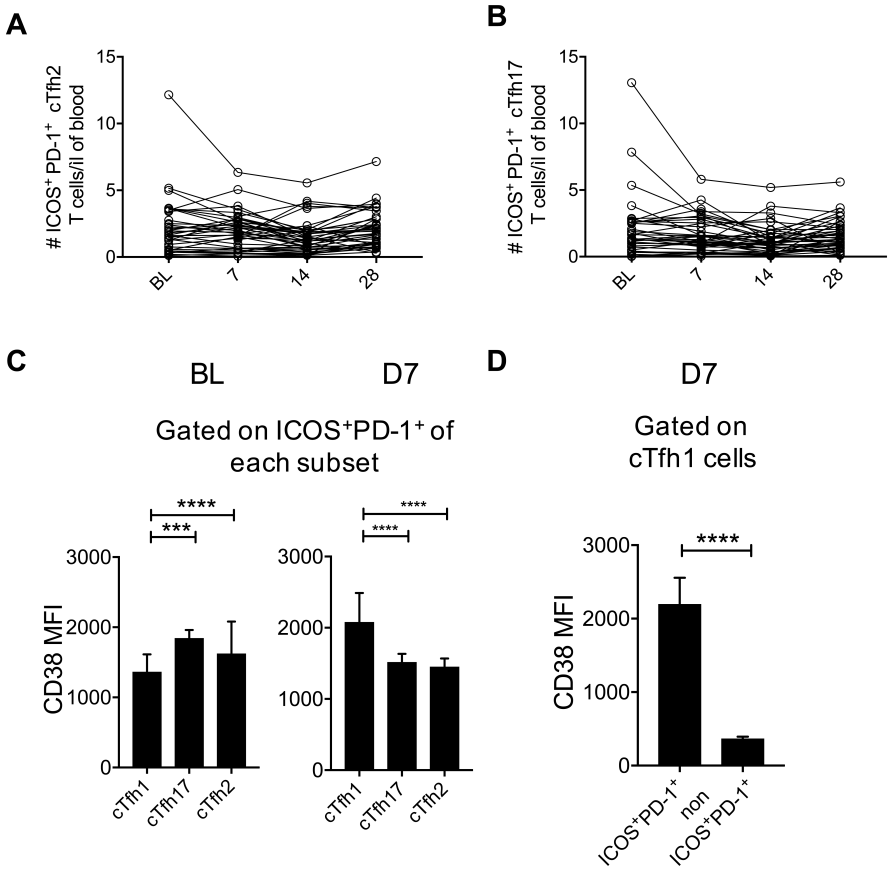

Fig S2. Specific activation of cTfh1 cells post-IIV. (A-B) Absolute numbers of activated ($ICOS^+PD\text{-}1^+$) cTfh2 (A) and cTfh17 (B) cells following vaccination (n=42, 2015 and 2016 cohorts). (C-D) CD38 expression was measured on different cTfh subsets. (C) CD38 expression on $ICOS^+PD\text{-}1^+$ cells of the three cTfh subsets at baseline (BL) and on day 7. (D) Expression of CD38 on $ICOS^+PD\text{-}1^+$ and non-$ICOS^+PD\text{-}1^+$ ($ICOS^-PD\text{-}1^{+/-}$) cTfh1 cells on day 7. cTfh1: $CXCR3^+CCR6^-$, cTfh2: $CXCR3^-CCR6^-$, cTfh17: $CXCR3^-CCR6^+$. Bars indicate the median, error bars indicate 95% confidence intervals, n=26 from the 2016 cohort. Statistical significance determined using Wilcoxon matched-pairs signed rank test (*P<0.05,**P<0.005, ***P<0.001. ****P<0.0001).

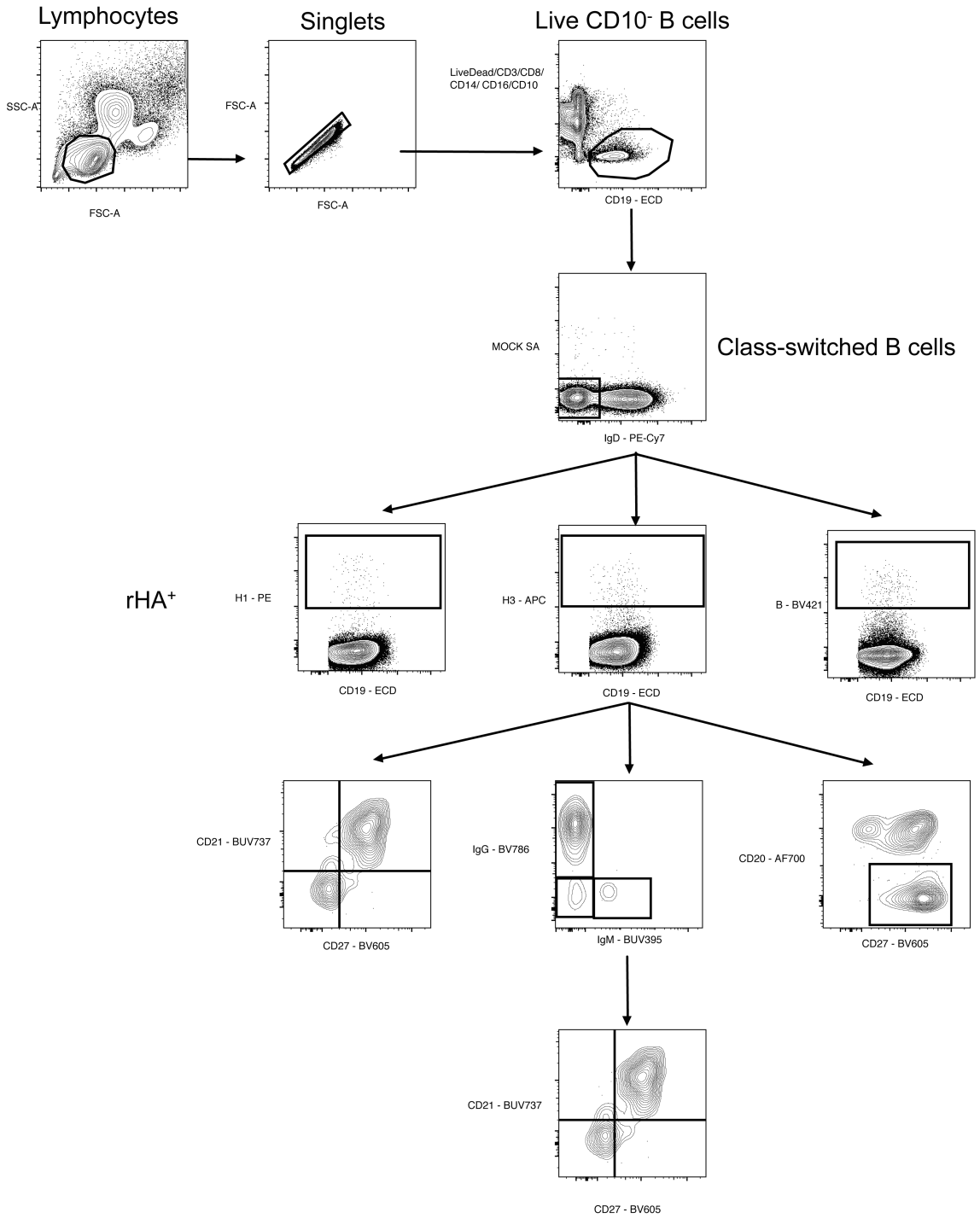

Fig S3. Gating strategy for influenza-specific B-cells in PBMC. Mature B cells were identified as live $CD19^{+}CD3^{-}CD8^{-}CD4^{-}CD14^{-}CD16^{-}CD10^{-}$ in single lymphocytes. B cells that bound free streptavidin-fluorochrome complexes were excluded from analysis. Influenza-specific B cells were identified as rHA^{+} cells within mature IgD^{-} B cells. rHA^{+} B cells were divided based on isotype expression and each isotype was divided into one of four phenotypes based on expression of CD21 and CD27.

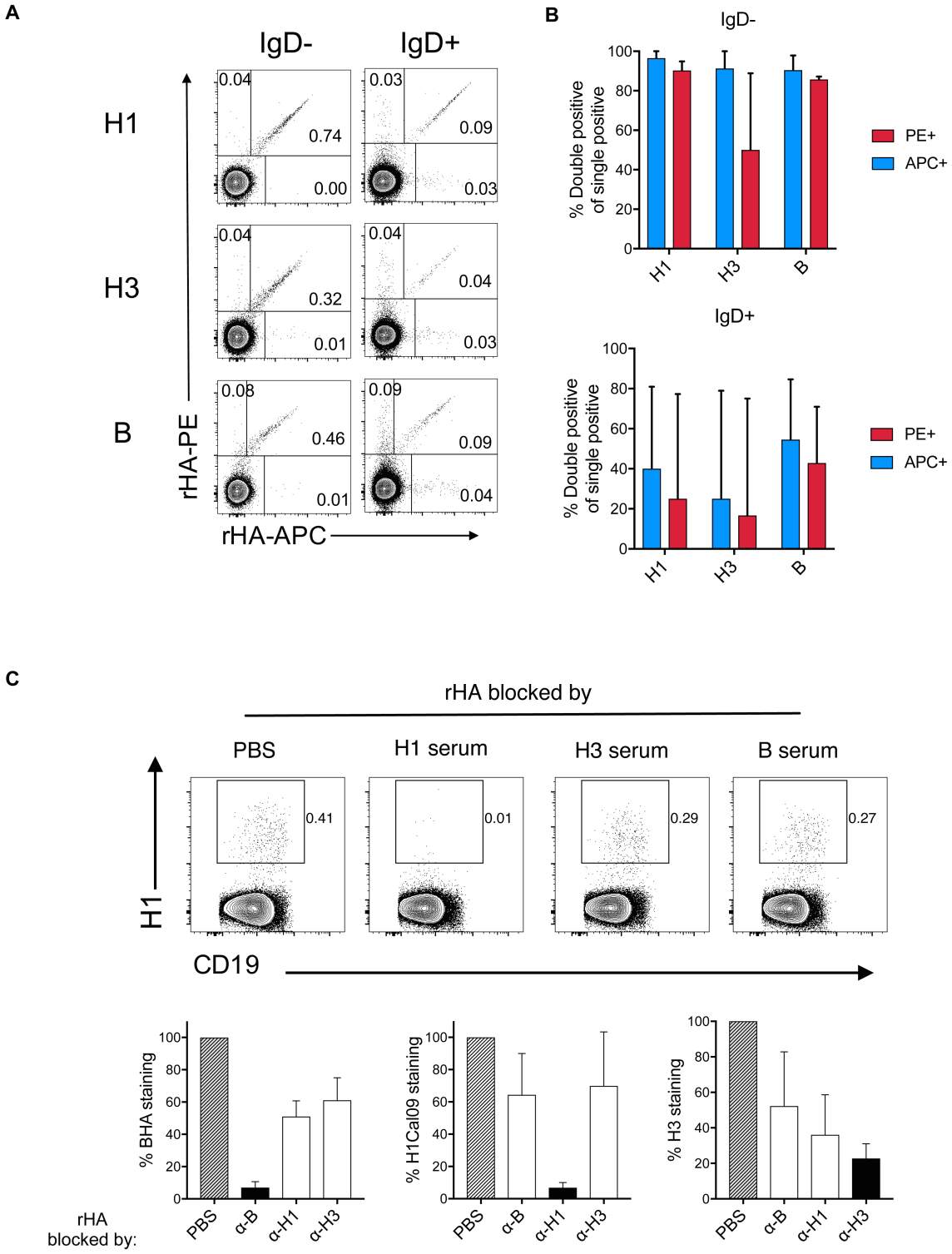

Fig S4. Validation of rHA probe staining. (A & B) Dual staining (with the same rHA probes conjugated to two fluorochromes, PE and APC) was used to confirm the specificity of single rHA$^+$ B cells. (A) Representative FACS plots are shown for IgD$^-$ and IgD$^+$ B cells for each rHA probe. (B) Percent of double positive rHA B cells within total single positive rHA+ B cells (eg. APC$^+$PE$^+$/APC$^+$ * 100) (n=5). (C-D) rHA staining blocking by cognate sheep anti-sera. rHA probes (H1-PE, H3-APC, BPHU-BV421) were incubate with individual sheep

antisera against each of the probes for 30mins at RT prior to staining PBMCs. (C) Representative FACS plots from one donors for the H1 probe are shown. (D) % of staining remaiing after blooking (relative to PBS treatment) is shown for each probe. Median with 95% confidence intervals are shown (n=4-5).

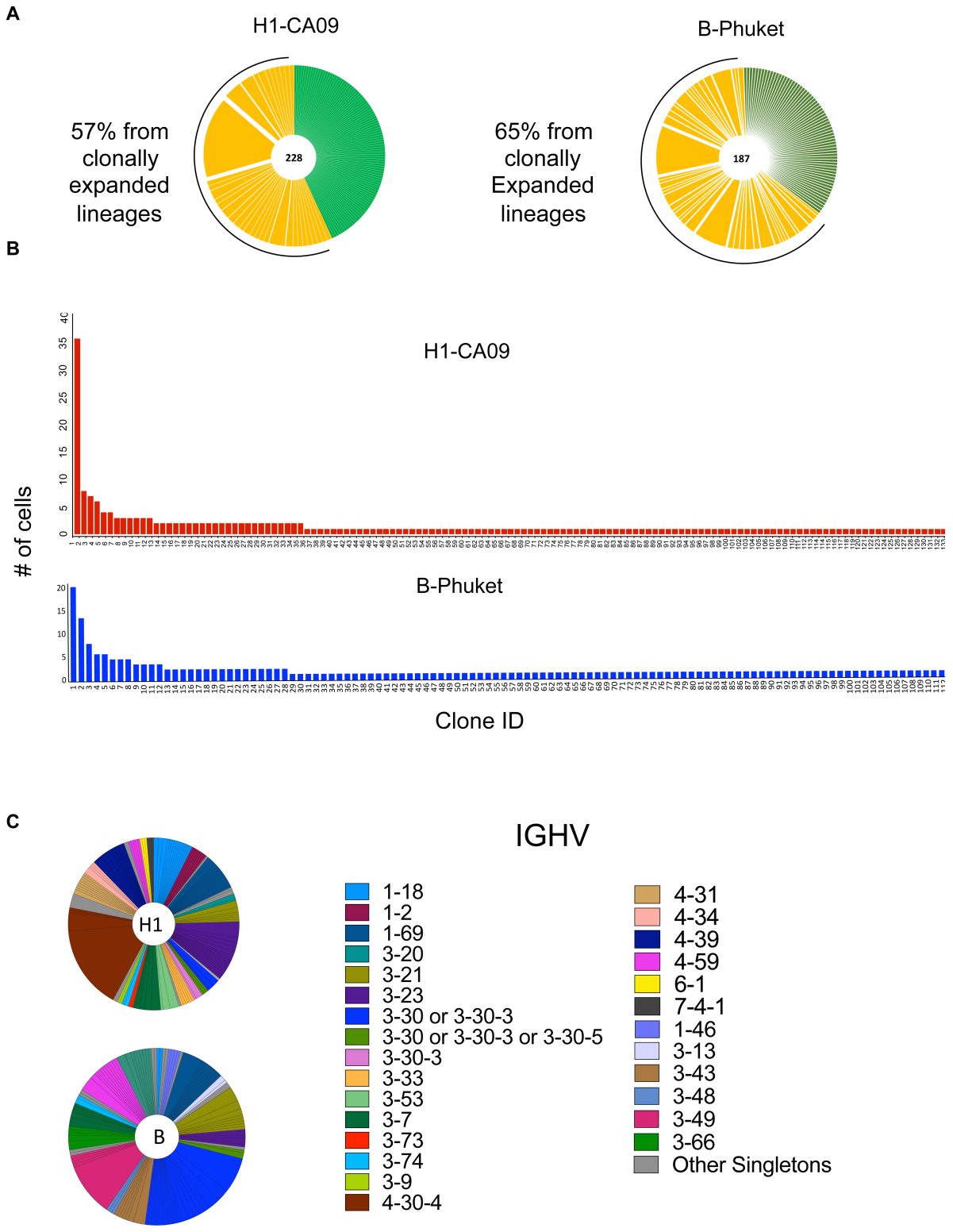

Fig S5. BCR analysis of single rHA$^+$B-cells. Single rHA$^+$ CD19$^+$ IgD$^-$ IgM$^-$ IgG$^+$ CD27$^+$ B cells were sorted directly *ex vivo* from PBMC samples and BCR sequences were recovered using a multiplex PCR approach. (A) Clonal expansions were analyzed based on IGHV usage and CDR3 sequence homology. The yellow segments indicate clonal expansions, with each

segment representing a different lineage. Green segments represent single clones. (B) Clonal distributions of $H1^+$ and B^+ sorted cells. (C) IGHV gene usage for $H1^+$ and B^+ cells. IGHV segments are color-coded. Pie-chart segment represent distinct clones as defined by CDR3 sequence homology. Pooled data from 3 donors.

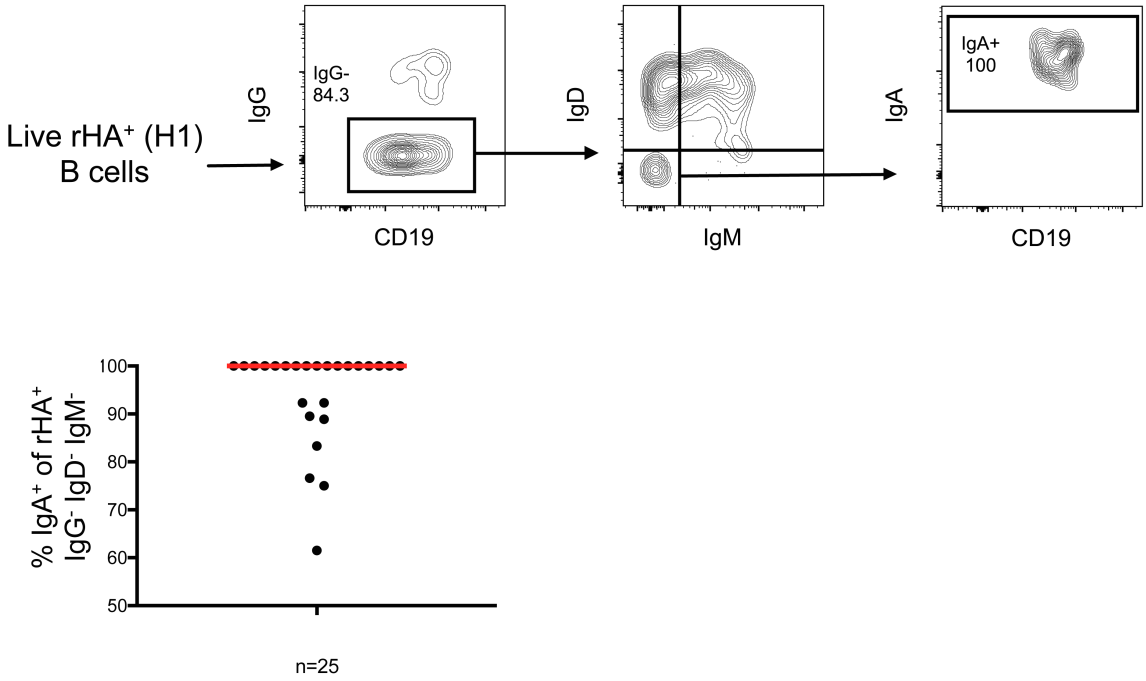

Fig S6. Frequency of IgA$^+$ cells in IgG$^-$D$^-$M$^-$rHA$^+$B-cells in healthy adults. PBMCs were stained using panel 4c (Table S8). IgA$^+$ rHA$^+$ (H1N1) cells were identified within the IgG-D-M- population. Line indicates the median (n=25).

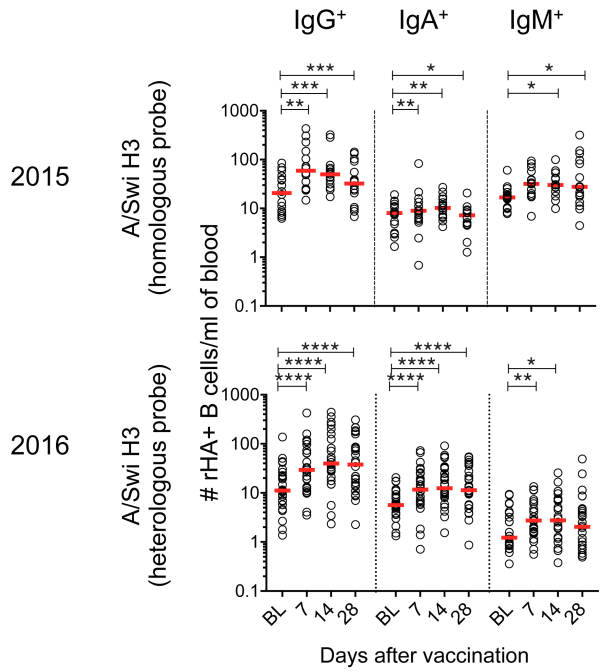

Fig S7. Numbers of isotype-specific rHA^{+}(H3N2\Swi) B-cells. 2015: n=16, 2016 n=26. Bars indicate the median. Statistical significance for changes from baseline was determined using Wilcoxon matched-pairs signed rank test (*P<0.05,**P<0.005, ***P<0.001. ****P<0.0001). Statistically significant comparisons are indicated.

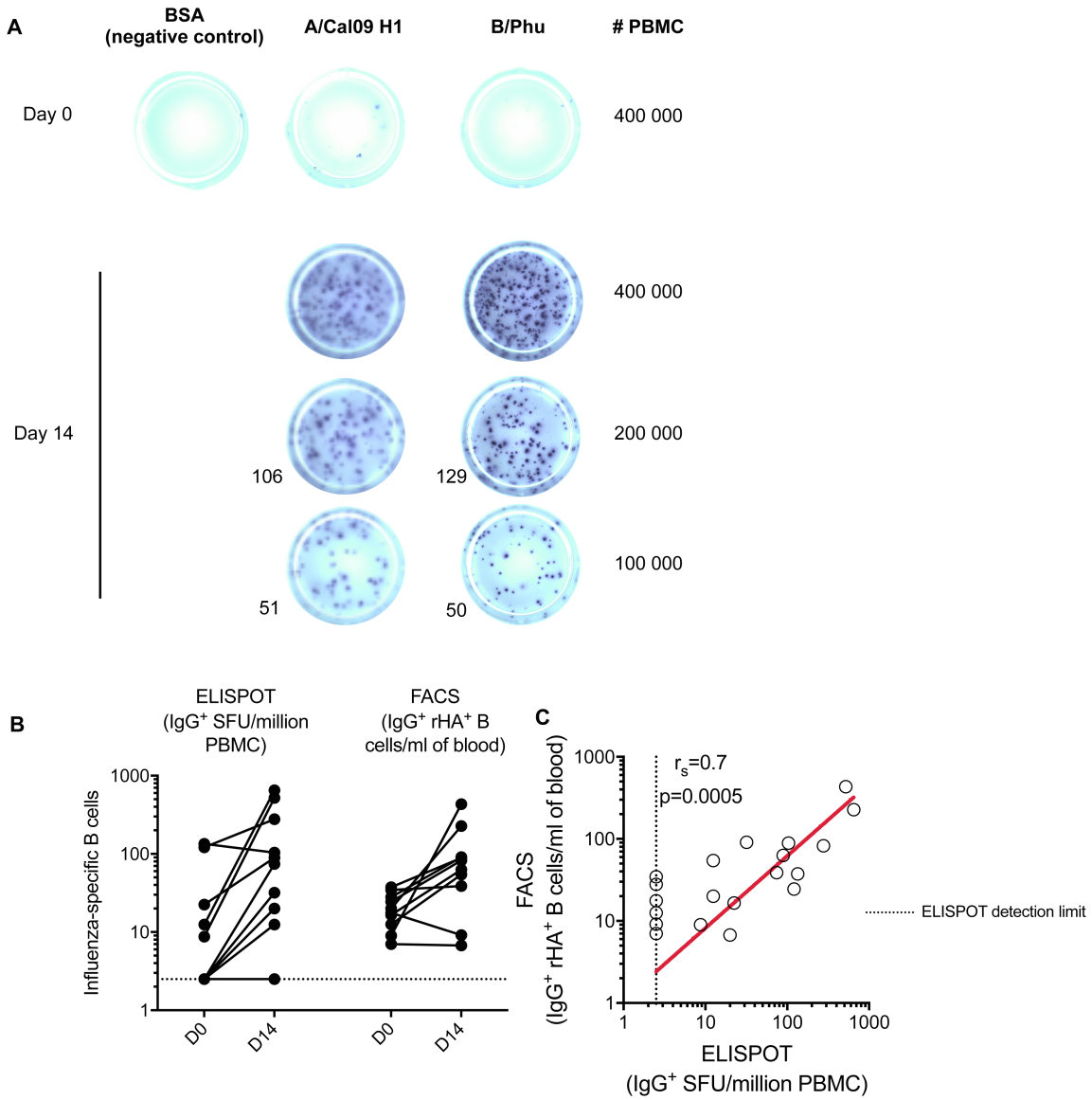

Fig S8. rHA$^+$B-cell kinetics by ELISPOTS. B cell responses were measured by IgG ELISPOT against inactivated purified influenza virus after 5 days of polyclonal stimulation. Samples from day 0 and day 14 after vaccination were used (n=5) and assessed against H1/Cal09 and B/Phu antigens. (A) Representative wells are shown from one donor. BSA was used as a negative control. (B) Kinetics of influenza specific B cells measured by ELISPOT (IgG spot forming units/million PBMC) or FACS (IgG$^+$rHA$^+$ B cells/ml of blood) are shown (pooled data for both H1 and B). (C) Correlation of numbers of influenza-specific B cells as measured by ELISPOT or FACS. Correlation was assessed by Spearman's correlation coefficient. Dotted line denoted the detection limit of our ELISPOT (1/400 000 PBMC). Negative wells were counted as the limits of detection.

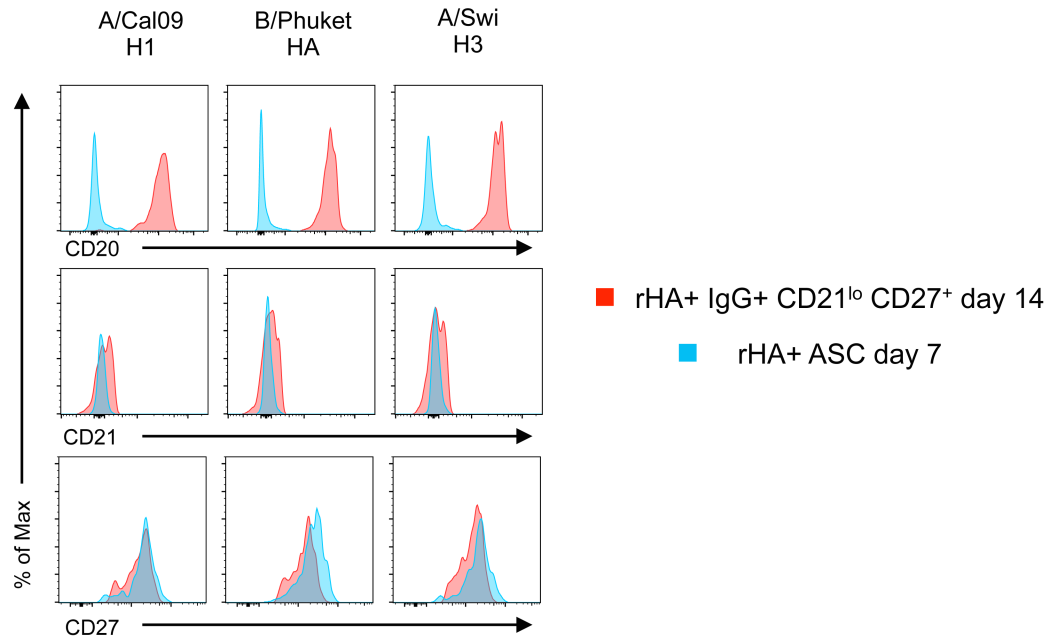

Fig S9. CD20 expression by CD21^{lo}CD27^{+}B-cells and ASCs. rHA^{+} B cells for each vaccine component were gated as **C**D21^{lo}CD27^{+} (day 14) or ASCs (CD20^{hi}CD27^{-} at day 7).

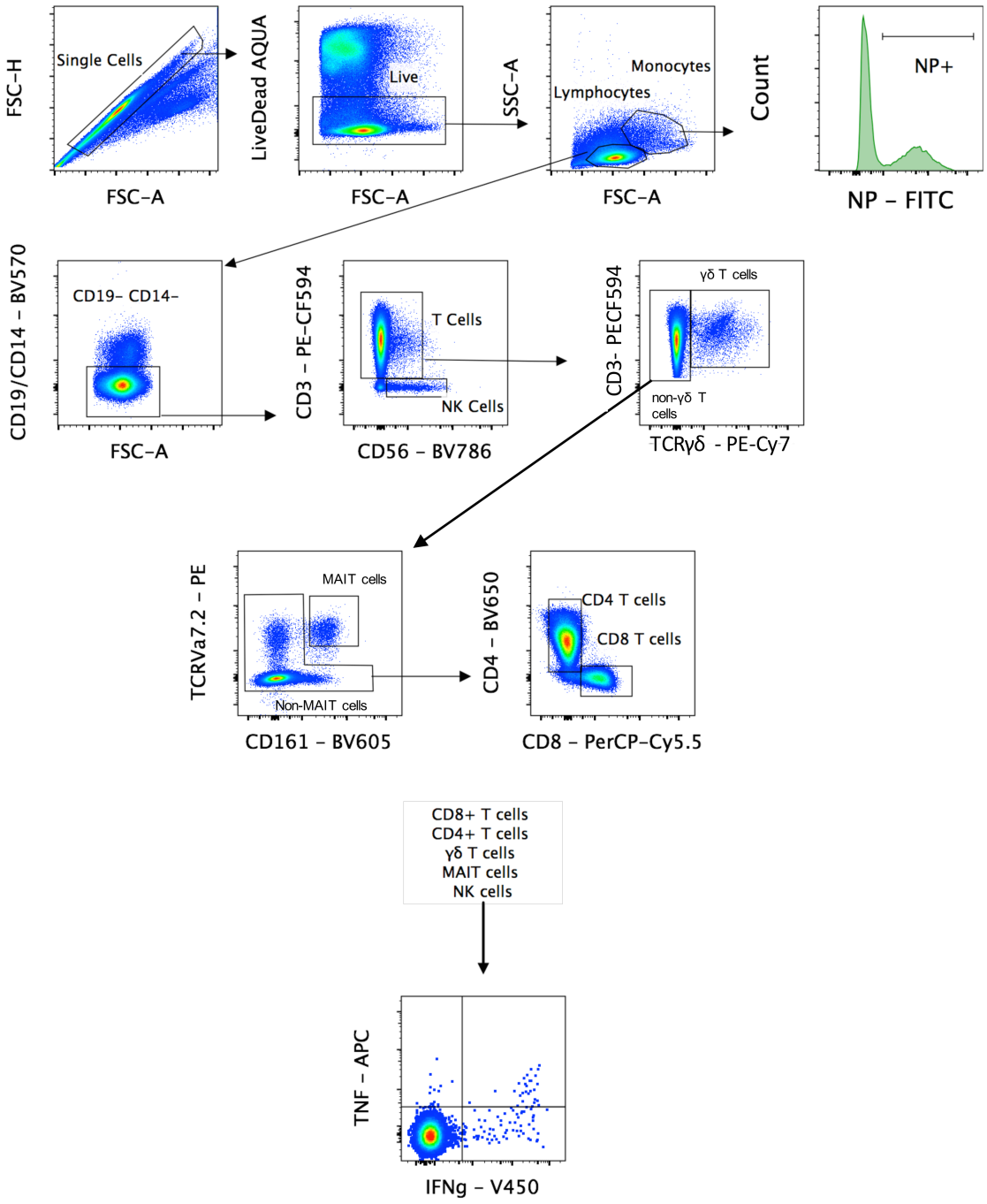

Fig. S10. Gating strategy for ex-vivo live virus ICS. Lymphocytes and monocytes were identified within single and live cells. Monocytes were assessed for IAV or IBV NP expression to assess infection rate. NK cells were identified as $CD56^{+}$ and T cells as $CD3^{+}$ within $CD19^{-}/CD14^{-}$ lymphocytes. γδ T cells were identified as γδ-TCR^{+} within T cells. MAIT cells were identified as $TCRVa7.2^{+}CD161^{+}$ within non- γδ T cells. $CD4^{+}$ and $CD8^{+}$ T cells were identified within non-MAIT cells. Influenza-specific/reactive lymphocytes were identified based on expression of IFNγ and TNF within each subset.

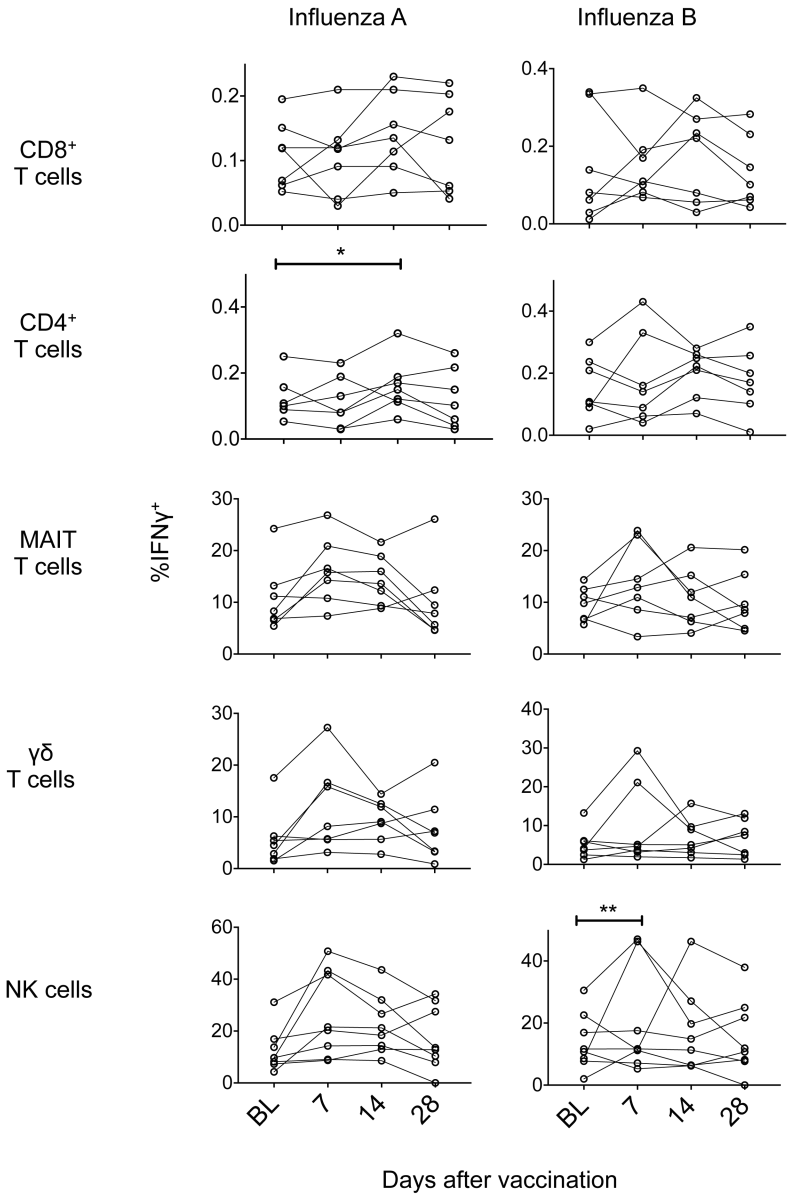

Fig. S11. Vaccination does not induce CD8$^+$ and innate T-cell responses. Frequencies of IFNγ^+ cells for each T cell subset stimulated with influenza A or B at different time-points (n=7). Data are displayed after subtracting the unstimulated (no virus) control. Statistical significance for changes between time-points was determined using the Friedman test. Statistically significant comparisons are indicated.

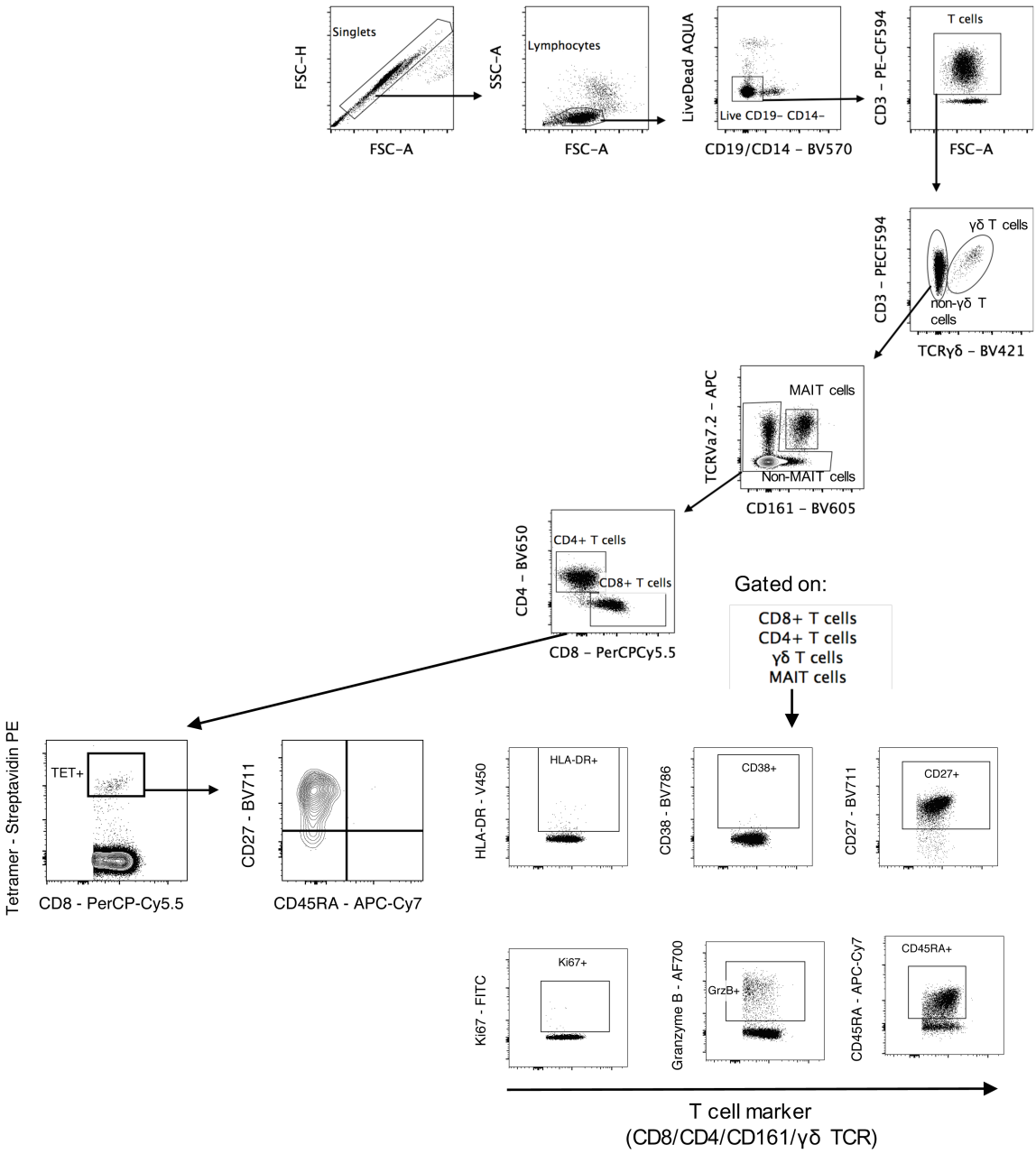

Fig. S12. Gating strategy for T-cell phenotyping. Lymphocytes were identified within single cells. T cells were identified as $CD3^+$ within live $CD19^-/CD14^-$ lymphocytes. γδ T cells were identified as γδ-TCR^+ within T cells. MAIT cells were identified as $TCRVa7.2^+CD161^+$ within non-γδ T cells. $CD4^+$ and $CD8^+$ T cells were identified within non-MAIT cells. Each subset was assessed for expression of HLA-DR, CD38, CD27, Ki-67, GrzB and CD45RA. $Tetramer^+$ cells were identified within $CD8^+$ T cells and assessed for expression of CD27 and CD45RA.

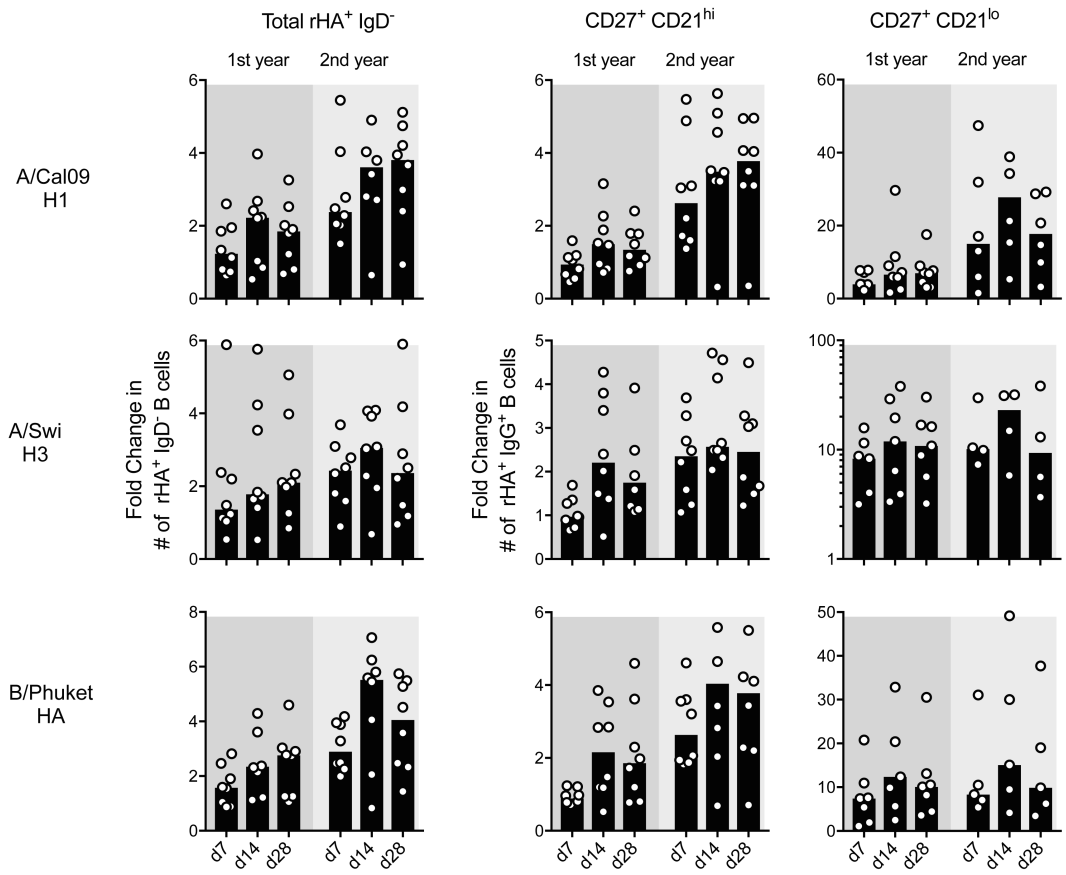

Fig S13. Fold-change in influenza-specific B-cells during repeated vaccination. (A-B) The B cell response of individuals vaccinated in both 2015 and 2016 was analysed by calculating the fold change at each time-point over the respective day 0. Fold change in (A) total IgD^- rHA^+ B cells and (B) $CD21^{hi}$ and $CD21^{lo}$ IgG^+ rHA^+ B cells are shown in the first and the second year after vaccination. Fold change was not calculated when day 0 measurement was 0.

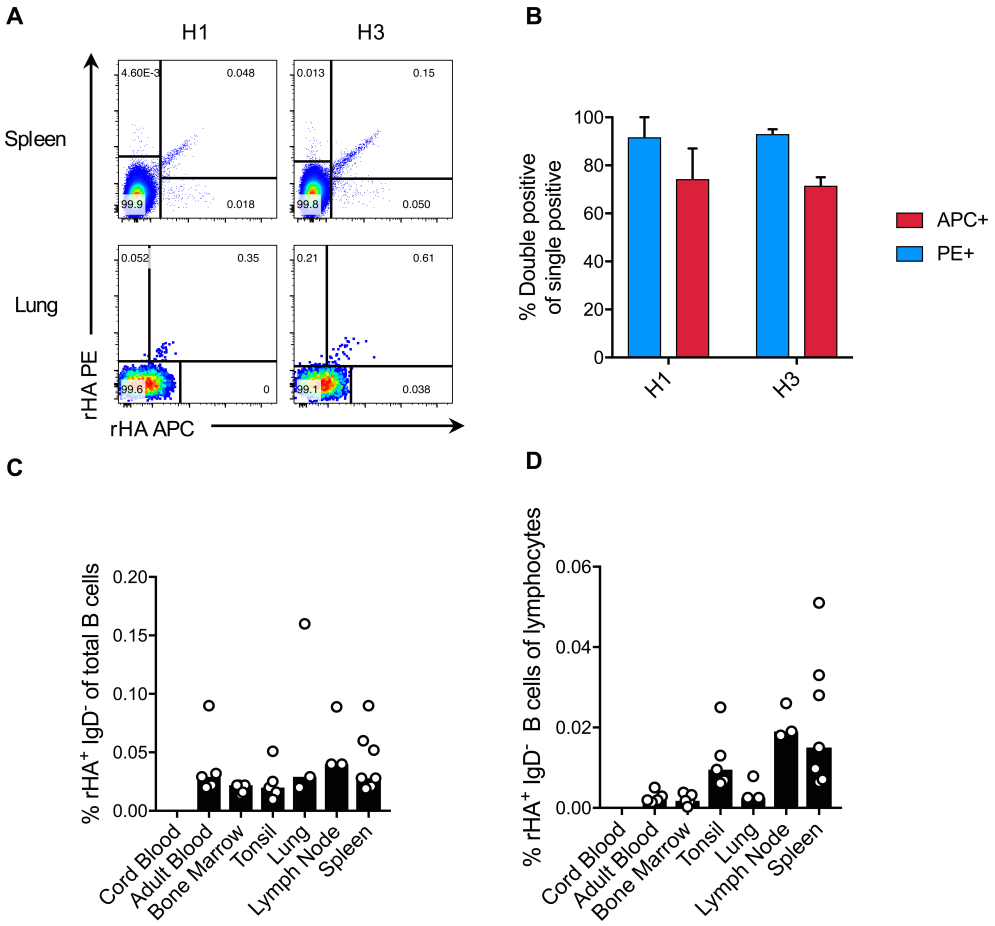

Fig S14. Validating of rHA probes in human tissues. Dual staining (with the same rHA probes conjugated to two fluorochromes, PE and APC) was used to confirm the specificity of single rHA^+ B cells. (A) Representative FACS plots are shown for H1 and H3 B cells in spleen and lung. (B) Percent of double positive rHA B cells within total single positive rHA^+ B cells (eg. $APC^+PE^+/APC^+ * 100$) (spleen n=5, lung n=1). (C) Frequency of rHA^+ IgD^- cells within B cells. (D) Frequency of rHA^+ IgD^- B cells within lymphocytes.

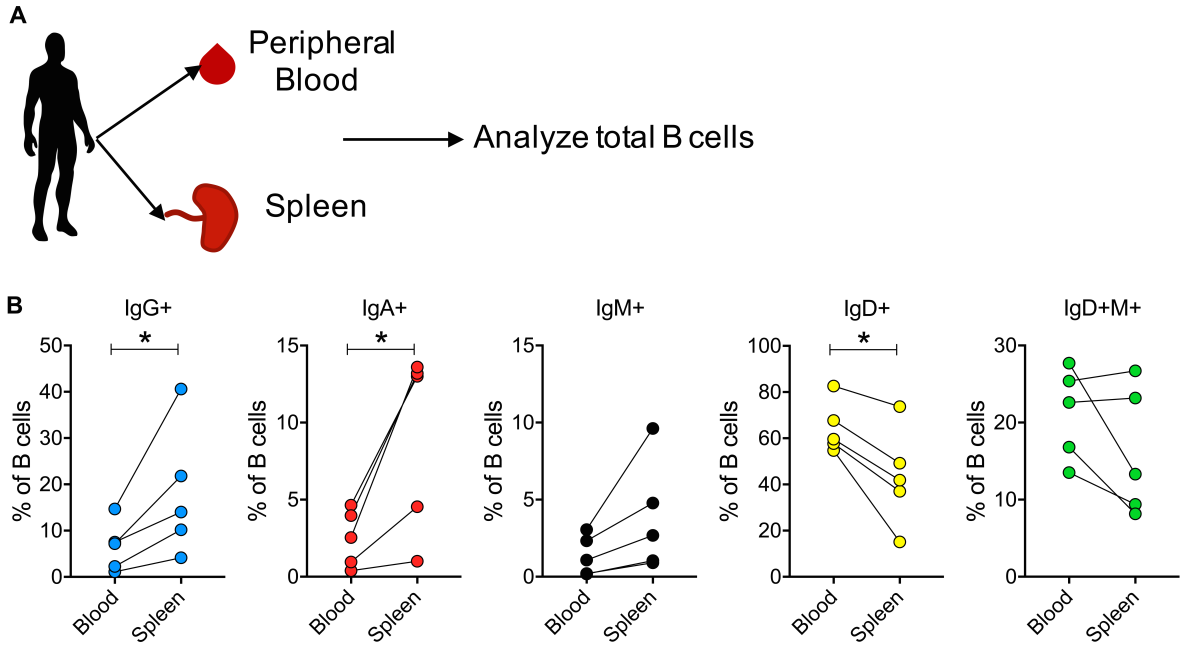

Fig S15. B-cell isotype distributions in paired tissue samples. (A) Mononuclear cells from paired peripheral blood and spleen samples were analyzed. (B) Frequency of each isotype within total B cells for each blood and spleen pair (n=5). Significance was assessed using a paired t-test (*P<0.05).

Study Code	Sex	Age*	HLA-A	HLA-B	2014	2105	2016
FV1	F	27	01:01, 26:01	08:01, 44:02	✖	✔	✖
FV2	M	30	01:01, 11:01	35:01, 52:01	✔	✖	✔
FV3	F	46	02:01, 03:02	18:01, 35:08	✖	✖	✔
FV4	F	25	1:01:01	8:01	✔	✔	✖
FV5	F	30	26:01, 33:03	40:02, 52:01	✔	✔	✖
FV6	F	28	ND	ND	✖	✔	✔
FV7	M	27	11:01, 26:01	14:01, 27:05	✖	✔	✔
FV8	F	31	02:07, 11:01	15:02, 57:01	✔	✔	✔
FV9	F	25	02:01, 02:03	38:02, 40:01	✔	✔	✔
FV10	M	29	11:01	40:01:00	✖	✖	✔
FV11	F	50	ND	ND	✖	✔	✔
FV12	F	31	02:01, 11:01	40:01, 44:02	✔	✖	✖
FV13	F	29	03:01:01, 33:03:01	35:01:01, 44:03	✖	✔	✔
FV14	M	34	ND	ND	✖	✔	✖
FV15	F	36	03:01, 31:01	07:02, 40:01	✖	✔	✔
FV16	F	41	ND	ND	✖	✔	✔
FV17	M	23	ND	ND	✖	✔	✖
FV18	M	24	33:03, 68:01	35:01, 58:01	✖	✖	✔
FV19	F	32	02:01, 11:01	40:01, 44:02	✔	✖	✖
FV20	M	27	11:01	38:02, 55:12	✖	✔	✔
FV21	M	31	02:01, 33:03	07:02, 27:02	✖	✔	✔
FV22	F	31	01:01, 03:01	7:02	✖	✔	✖
FV23	F	47	ND	ND	✖	✔	✔
FV24	F	25	ND	ND	✖	✖	✔
FV25	M	55	ND	ND	✖	✖	✔
FV26	F	48	ND	ND	✖	✖	✔
FV27	F	22	ND	ND	✖	✖	✔
FV28	F	52	ND	ND	✖	✖	✔
FV29	F	22	ND	ND	✖	✖	✔
FV30	F	22	ND	ND	✖	✖	✔
FV31	F	46	ND	ND	✖	✖	✔
FV32	F	36	ND	ND	✖	✖	✔
FV33	F	25	ND	ND	✖	✖	✔
FV34	F	22	ND	ND	✖	✖	✔
FV35	F	29	ND	ND	✖	✖	✔

Table S1. Details of vaccination cohorts.

Tissue	Donor Code	Gender	Age	Status	Casue of Death	Sampling year
Peripheral Bloood	BP1	F	31	Healthy	N/A	2016
	BP2	M	68	Healthy	N/A	2016
	BP3	F	50	Healthy	N/A	2016
	BP4	F	46	Healthy	N/A	2016
	BP5	F	57	Healthy	N/A	2016
Cord Blood	CB1	Unknown	0	Healthy	N/A	2016
	CB2	Unknown	0	Healthy	N/A	2016
	CB3	Unknown	0	Healthy	N/A	2016
	CB4	Unknown	0	Healthy	N/A	2016
	CB5	Unknown	0	Healthy	N/A	2016
Bone Marrow	BM1	M	33	Healthy	N/A	2015
	BM2	M	45	Healthy	N/A	2009
	BM3	F	35	Healthy	N/A	2009
	BM4	M	34	Healthy	N/A	2009
	BM5	M	43	Healthy	N/A	2009
Tonsil	TNS1	M	30	Healthy	N/A	2014
	TNS2	M	38	Healthy	N/A	2014
	TNS3	M	24	Healthy	N/A	2014
	TNS4	F	3	Healthy	N/A	2014
	TNS5	F	16	Healthy	N/A	2014
Spleen	SP1	M	65	Deceased	Cerebral infarction	2016
	SP2	M	61	Deceased	Intracranial haemorrhage	2016
	SP3	M	69	Deceased	Intracranial haemorrhage	2016
	SP4	M	49	Deceased	Traumatic brain injury (fall)	2016
	SP5	F	28	Deceased	Traumatic brain injury (MVA)	2016
	SP6	F	57	Deceased	Intracranial haemorrhage	2016
	SP7	M	57	Deceased	Intracranial haemorrhage	2016
Lymph Node	mLN1	F	28	Deceased	Traumatic brain injury (MVA)	2016
	mLN2	F	38	Deceased	Intracranial haemorrhage	2016
	pLN1	M	53	Deceased	Traumatic brain injury (MVA)	2016
Lung	LNG1	M	61	Deceased	N/A	2016
	LNG2	M	41	Deceased	N/A	2015
	LNG4	M	50	Deceased	N/A	2015

Paired tissue samples				
Donor	**Age**	**Status**	**Casue of Death**	**Sampling year**
PS1	18	Deceased	N/A	2009
PS2	45	Deceased	N/A	2014
PS3	36	Deceased	N/A	2014
PS4	71	Deceased	N/A	2014
PS5	70	Deceased	N/A	2014

N/A=Not applicable
MVA=motor vehicle accident

Table S2. Cohorts of human tissues.

PANEL 1 (Whole blood B/Tfh)				
Antibody	**Clone**	**Fluorochrome**	**Dilution**	**Vendor**
CD8	OKT8	FITC	1:25	eBioscience
CD45	2D1	PerCP-Cy5.5	1:50	BD
CXCR3	1C6	APC	1:25	BD Pharmingen
CD27	O323	AF700	1:50	eBioscience
CD4	RPAT4	APC-H7	1:100	BD
CXCR5	RF8B2	BV421	1:50	BD Horizon
CD19	HIB19	BV570	1:200	Biolegend
CD24	MLS	BV605	1:100	BD Horizon
CCR6	11A9	BV650	1:100	BD Horizon
CD20	2H7	BV711	1:200	BD Horizon
CD38	HIT2	BV786	1:400	BD Horizon
ICOS	DX29	PE	1:10	BD Pharmingen
CD3	UCHT1	PECF594	1:400	BD
PD1	EH12.1	PE-Cy7	1:100	BD Pharmingen

Table S3. FACS panel for ASCs and cTfh cells.

PANEL 2 (Virus ICS)				
Antibody	**Clone**	**Fluorochrome**	**Dilution**	**Vendor**
FLUA NP (intracellular)	1331	FITC	1:200	GeneTex
FLUB NP (intracellular)	H89B	FITC	1:200	ThermoFisher
CD8	SK1	PerCP-Cy5.5	1:50	BD
TNF (intracellular)	6401.1111	APC	1:100	BD
CD19	SJ25C1	APC-H7	1:100	BD Pharmingen
CD14	MΦP9	APC-H7	1:100	BD Pharmingen
IFNγ (intracellular)	B27	V450	1:100	BD Horizon
Live Dead	N/A	AQUA	1:500	ThermoFisher
CD161	HP-3G10	BV605	1:50	Biolegend
CD4	SK3	BV650	1:200	BD Biosciences
CD56	NCAM16.2	BV786	1:100	BD Horizon
TCR-Vα7.2	3C10	PE	1:400	icyt
CD3	UCHT1	PECF594	1:200	BD
TCRγδ	11F2	PE-Cy7	1:50	BD

Table S4. FACS panel for influenza-specific T-cells after influenza virus infection.

Panel 3 (T cell phenotype)				
Antibody	**Clone**	**Fluorochrome**	**Dilution**	**Vendor**
Ki-67 (intracellular)	MOPC-21	FITC	1:10	BD Pharmingen
CD8	SK1	PerCP-Cy5.5	1:50	BD
TCR-Vα7.2	3C10	APC	1:50	icyt
Granzyme B (intracellular)	GB11	AF700	1:50	BD Pharmingen
CD45RA	HI100	APC-H7	1:50	BD Pharmingen
HLA-DR	L243	V450	1:200	BD
Live Dead	N/A	AQUA	1:500	ThermoFisher
CD19	HIB19	BV570	1:200	Biolegend
CD14	ME2	BV570	1:200	Biolegend
CD161	HP-3G10	BV605	1:50	Biolegend
CD4	SK3	BV650	1:200	BD Biosciences
CD38	HIT2	BV786	1:400	BD Horizon
Tetarmer	N/A	PE	1:200	N/A
CD3	UCHT1	PECF594	1:200	BD
TCRγδ	11F2	PE-Cy7	1:50	BD

Table S5. FACS panel for phenotyping T-cells after vaccination.

Panel 4a (HA B cells 2015)				
Antibody	**Clone**	**Fluorochrome**	**Dilution**	**Vendor**
Free SA	N/A	BB515	1:600	BD Horizon
H3 rHA	N/A	APC	N/A	N/A
CD20	2H7	AF700	1:150	BD
BPHU	N/A	BV421	N/A	N/A
Live Dead	N/A	AQUA	1:500	ThermoFisher
CD3	OKT3	BV510	1:600	Biolegend
CD8	RPA-T8	BV510	1:1500	Biolegend
CD10	HI10a	BV510	1:750	Biolegend
CD14	M5E2	BV510	1:300	Biolegend
CD16	3G8	BV510	1:500	Biolegend
CD27	O323	BV605	1:150	Biolegend
IgG	G18-145	BV786	1:75	BD
H1 rHA	N/A	PE	N/A	N/A
CD19	J3-119	ECD	1:150	Beckman
IgD	IA6-2	PE-Cy7	1:500	BD
IgM	G20-127	BUV395	1:150	BD
CD21	B-ly4	BUV737	1:300	BD

Table S6. FACS panel for influenza-specific B-cells in 2015-cohort.

Panel 4b (HA B cells 2016)				
Antibody	**Clone**	**Fluorochrome**	**Dilution**	**Vendor**
Free SA	N/A	BV510	1:600	BD Horizon
H3 rHA	N/A	APC	N/A	N/A
CD20	2H7	AF700	1:150	BD
BPHU	N/A	BV421	N/A	N/A
Live Dead	N/A	AQUA	1:500	ThermoFisher
CD3	OKT3	BV510	1:600	Biolegend
CD8	RPA-T8	BV510	1:1500	Biolegend
CD10	HI10a	BV510	1:750	Biolegend
CD14	M5E2	BV510	1:300	Biolegend
CD16	3G8	BV510	1:500	Biolegend
CD27	O323	BV605	1:150	Biolegend
IgG	G18-145	BV786	1:75	BD
H1 rHA	N/A	PE	N/A	N/A
CD19	J3-119	ECD	1:150	Beckman
IgD	IA6-2	PE-Cy7	1:500	BD
IgM	G20-127	BUV395	1:150	BD
CD21	B-ly4	BUV737	1:300	BD

Table S7. FACS panel for influenza-specific B-cells in 2016-cohort.

Panel 4c (HA Tissue B cells)				
Antibody	**Clone**	**Fluorochrome**	**Dilution**	**Vendor**
Free SA	N/A	BV510	1:600	BD Horizon
H3 rHA	N/A	APC	N/A	N/A
CD20	2H7	AF700	1:150	BD
IgA	IS11-8E10	VioBlue	1:150	Miltenyi Biotec
Live Dead	N/A	AQUA	1:500	ThermoFisher
CD3	OKT3	BV510	1:600	Biolegend
CD8	RPA-T8	BV510	1:1500	Biolegend
CD10	HI10a	BV510	1:750	Biolegend
CD14	M5E2	BV510	1:300	Biolegend
CD16	3G8	BV510	1:500	Biolegend
CD27	O323	BV605	1:150	Biolegend
IgG	G18-145	BV786	1:75	BD
H1 rHA	N/A	PE	N/A	N/A
CD19	J3-119	ECD	1:150	Beckman
IgD	IA6-2	PE-Cy7	1:500	BD
IgM	G20-127	BUV395	1:150	BD
CD21	B-ly4	BUV737	1:300	BD

Table S8. FACS panel for influenza-specific B-cells in human tissues.